DEMOCRATIC AND POPULAR ALGERIAN REPUBLIC
MINISTRY OF HIGHER EDUCATION AND SCIENTIFIC RESEARCH

University of Blida 1

The Institute of Aeronautics and Space studies

In view of obtaining the Master's Degree
Branch: **Aeronautics**
Option:**Avionics**

FORMATION CONTROL FOR A SWARM OF UNMANNED AERIAL VEHICLES

Presented by	**In front of the jury**	
Mme.AZIKIOU Nassima	Dr.CHOUTRI	Supervisor
Mme.ZIANE Meriem	Pr.LAGHA	Co-supervisor
	Pr.KOUIDER	Examiner
	Dr.DILMI	Examiner

Promotion: 2019-2020

Acknowledgements

We would like to thank first and foremost the Lord God Almighty for his never ending grace.

At the end of this work, we would like to thank, enormously, all those who participated in the elaboration of this final thesis. May they find here our deepest gratitude.

First, we address our sincere thanks to our promoter, Doctor CHOUTRI Kheireddine and Doctor LAGHA, for having always trusted us in the way of carrying out our work. We also thank him for his availability, his help, his support and his human qualities.

Our most sincere gratitude to the teachers of the Avionics department, and of IAES in general, thanks to whom we have been able to reach this point.

Dedications

To my dear parents, whose merit, sacrifices and human qualities allowed me to live this day. No dedication could be eloquent enough to express what you deserve for all the sacrifices you have never ceased to give me since my birth. I dedicate this work to you as a testimony of my deep love. May God, the Almighty, preserve and grant your health, long life and happiness.

To my brothers and sisters, for their love and unquestionable support.

To all my family, I dedicate this work to all the people dear to my heart. May they find here the expression of all my gratitude and love.

To all my friends, a special and sincere thank you for all your efforts. You have always been present. May this work be a testimony of my gratitude and my deep respect.

Azikiou Nassima,Ziane Mariem

ABSTARCT

In this thesis, we have been concerned with the problems of the formation control strategies of multiple quadrotors.

First of all, the mathematical model of a quadrotor UAV was developed in details including its aerodynamic effects and DC motor which we found lacking in many literatures. A control technique was then developed and synthesized; which is the linear Proportional-Integral-Derivative (PID) controller. A complete simulation was then implemented on MATLAB/Simulink relying on the derived mathematical model of the quadrotor. The simulation environment was used to evaluate the performances of the mentioned controller.

After that, the path planning and obstacle avoidance for a single quadrotor has been investigated. For that the ACO algorithm was chosen to generate the shortest path from the initial position to the final destination, the simulation environment was MATLAB as well. The same controller was used in this phase to track the generated path.

Finally, we were concerned to the problem of the quadrotors swarming formation control. Three formation control strategies were proposed, and the centralized Leader-followers formation was the chosen strategy to solve the problem.

Keys words: Quadrotor, Multi-UAVs, PID controller, Path planning Obstacles Avoidance, ACO, Formation control.

الملخص

في الآونة الأخيرة، تحظى الطائرات بدون طيار (UAVs) بمزيد من الاهتمام من الباحثين في كل من التطبيقات المدنية والعسكرية. أصبحت طائرات الهليكوبتر الرباعية بشكل خاص مستخدمة على نطاق واسع في أحدث الأبحاث نظرًا لقدرتها على الإقلاع والهبوط العمودي (VTOL). ساعدتهم هذه الخاصية على تحقيق مهامهم بنجاح في العديد من التطبيقات مثل البحث والاستكشاف والاستطلاع والمراقبة ومكافحة الحرائق. ورغم انه يمكن تنفيذ هذه المهام بمركبة واحدة فقط، لكن ستكون المركبات المتعددة أكثر مرونة وكفاءة ولديها قدر أكبر من تحمل الأعطال في أداء المهمة.

كما ذُكر سابقا، فإن استخدام عدة طائرات بدون طيار هو أكثر فاعلية ولكن من ناحية أخرى فإن التحكم فيها أكثر تعقيدًا وصعوبة من التحكم في طائرة واحدة. لحل هذه المشكلة، يجب أن تحافظ مجموعة الطائرات بدون طيار على شكل تشكيل معين مع مسافات نسبية ثابتة بينها.

الكلمات المفتاحية :طائرة رباعية المراوح، مجموعة الطائرات بدون طيار، وحدة تحكم PID، تخطيط المسار وتجنب العقبات، خوارزمية ACO، التحكم في التشكيل.

LIST OF TABLES

LIST OF FIGURES

LIST OF SYMBOLS

$\boldsymbol{allow_k}$:the collection of grids

$\boldsymbol{C_D}$:aerodynamic drag coefficient

$\boldsymbol{C_k}$: the total path length

$\boldsymbol{C_T}$: aerodynamic thrust coefficient

$\boldsymbol{e}$: Error

$\boldsymbol{F_b}$: nongravitational forces acting on the quadrotor

$\boldsymbol{I}$: Identity matrix

$\boldsymbol{i}$:motor current

$\boldsymbol{I_{xx}}$: Area moment of inertia about the x-axis

$\boldsymbol{I_{yy}}$: Area moment of inertia about the y-axis

$\boldsymbol{I_{zz}}$: Area moment of inertia about the z-axis

J:Quadrotor's diagonal inertia matrix

$\boldsymbol{j}$: generic index

$\boldsymbol{J_R}$: rotor's inertia

g: gravitational acceleration g =9.81m/s^2

$\boldsymbol{k}$:generic index

$\boldsymbol{k_d}$:Derivative gain

$\boldsymbol{K_F}$: aerodynamic force constant

$\boldsymbol{k_i}$: Integral gain

$\boldsymbol{K_M}$:aerodynamic moment constant

$\boldsymbol{k_p}$: Proportional gain

$\boldsymbol{K_r}$: aerodynamic rotation coefficient matrix

$\boldsymbol{K_T}$: aerodynamic translation coefficient matri

$\boldsymbol{l}$:moment arm

$\boldsymbol{m}$:mass of quadrotor

$\boldsymbol{M_B}$: moments acting on the quadrotor in the body frame

$\boldsymbol{n}$: number of data acquired

$\boldsymbol{P_E}$:electric motor power

$\boldsymbol{P_M}$: mechanic motor power

$\boldsymbol{P_P}$:mechanic propeller power

R: Rotation Matrix

$\boldsymbol{r}$**:** Quadrotor's position in the navigation frame

$\boldsymbol{T_L}$: load torque

$\boldsymbol{T_M}$:motor torque

$\boldsymbol{T_{PM}}$:motor torque on propeller axis

$\boldsymbol{U}$**:** Control input vector

v : input motor voltage

$\boldsymbol{v_L}$ **:**motor inductance voltage

$\boldsymbol{v_R}$ **:** motor resistance voltage

X: State vector

$\boldsymbol{x_d}$:Desired x position

$\boldsymbol{y_d}$: Desired y position

$\boldsymbol{z_d}$: Desired altitude z

α: the stimulating factor of pheromone concentration

β: the stimulating factor of visibility.

$\boldsymbol{\rho}$:the evaporation rate of the pheromone

$\boldsymbol{\Omega}$:propellers' speed vector

$\boldsymbol{\Omega_1}$:front propeller speed

$\boldsymbol{\Omega_2}$:right propeller speed

$\boldsymbol{\Omega_3}$:rear propeller speed

$\boldsymbol{\Omega_4}$: left propeller speed

$\boldsymbol{\Omega_h}$: Hover angular velocity

$\boldsymbol{\Omega_n}$:speed of rotor n

$\boldsymbol{\Omega_r}$: rotors' relative speed

$\dot{\boldsymbol{\Omega}}$: propellers' acceleration vector

$\dot{\boldsymbol{\eta}}$: Euler rates

$\boldsymbol{\omega}$ **:** Angular body rates

$\boldsymbol{\theta}$ **:** roll angle

$\boldsymbol{\theta_d}$: Desired roll θ

$\boldsymbol{\psi}$: yaw angle

$\boldsymbol{\psi_d}$: Desired yaw

$\boldsymbol{\rho}$ **:**air density

$\boldsymbol{\phi}$ **:** pitch angle

$\boldsymbol{\phi_d}$ **:** Desired pitchϕ

$\boldsymbol{\omega_M}$:motor speed

$\dot{\omega}_M$:motor acceleration

ω_p:propeller speed

$\dot{\omega}_p$:propeller acceleration

τ_{ij}:the pheromone trail of the path grid i to grid j

ηij: the heuristic information of the path grid i to grid j

$\tau_{ij}(t)$:represents the residual amount of a path pheromone found by the ant after volatilization

$\Delta\tau_{ij}^{k}$: the pheromone left by the k^{th} ant in the path i to j

ACRONYMS:

ACE : Autonomous Control Engineering

ACO : Ant Colony Optimization

DASI : Digital Array Scanned Interferometer

DAST : Drones for Aerodynamic and Structural Testing

DOF : Degrees of Freedom

EC : Environmental Complexity

ERAST : Environmental Research Aircraft and Sensor Technology Project

HALE : High-Altitude Long-Endurance

HI : Human Independence

HiMAT : Highly Maneuverable Aircraft Technology

IMU : Inertial Measurement Unit

MALE: Medium-Altitude Long-Endurance

MC : Mission Complexity

MAS : Multi-agent system

MAV: Micro UAV

MUAV : Mini UAV

MEMS/NEMS : Micro and Nano-Electro-Mechanical-Systems

NAV : Nano Air Vehicles

SOS : Systems of systems

SMC : Sliding Mode Controller

TUAV: Tactical UAV

PD : Proportional-Derivative

PID : Proportional-Integral-Derivative

UAV : Unmanned Aerial Vehicle

VTOL : Vertical Takeoff and Landing

WWI : World War I

1 Sommaire

GENERAL INTRODUCTION

Flying objects have always exerted a great fascination on man encouraging all kinds of research and development. The scientific challenge in MAV design and control in cluttered environments and the lack of existing solutions was very motivating. In addition, The cooperation of multiple quadrotors is promising in order to accomplish complex tasks that are impossible to be completed by a single quadrotor.

This thesis presents a global version on UAVs (uses, classifications,types…) and precisely on quadrotors, which details in its mathematical modelling based on Newton Euler formalism. Besides that a control algorithmis devlopped to stabilize the quadrotor movements, this controller is going to be implemented on MATLAB/Simulink to asses its performance.the path planning and obstacle avoidane for a single quadrotor using a specific algorithm.Finally, a formation control strategies for a multi qudrotor system is studied, and the goal of this thesis is reached.

I. CHAPTER : GENERALITIES ABOUT DRONES

I.1 INTRODUCTION

In this chapter a brief introduction about Unmanned Aerial Vehicles (UAVs), their history, types and uses will be presented. Then move to the quadrotor type UAVs and discuss their concept and architecture. After that we will see what's the formation control of multiples quadrotors and why we need this last one. Lastly, the structure of the thesiswillbeoutlined.

I.2 OVERVIEW OF UNMANNED AERIAL VEHICLES

The definition for UAVs varies from one literature to the other. For our purposes, UAVs are small aircrafts that are own without a pilot. They can either be remotely operated by a human or they can be autonomous; autonomous vehicles are controlled by an onboard computer that can be preprogrammed to perform a specific task or a broad set of tasks. While in other literatures, UAVs may refer to powered or unpowered, tethered or untethered aerial vehicles (1). The definition used in this thesis is based on that of the American Institute of Aeronautics and Astronautics (1):

> An aircraft which is designed or modified not to carry a human pilot and
> is operated through electronic input initiated by the flight controller or
> by an on board autonomous flight management control system that does
> not require flight controller intervention.

UAVs were mainly used in military application but recently they are being deployed in civil applications too (2).

I.2.1 HISTORY OF UAVS

UAVs were first manufactured by Lawrence and Sperry (USA) in the year 1916. They called it the Aviation Torpedo shown in Figure I-1 and they were able to y it for a distance of 30 miles. It was reported that Lawrence and Sperry used a gyroscope to balance the body (2).

Figure I-1: Lawrence and Sperry UAV (2)

I.2.1.1 MILITARY HISTORY

A great interest was shown by the USA to develop UAVs to be used in the World War I (WWI) and two projects where funded. The first was by Elmer Sperry to develop the \Flying Bomb" UAV and the second project was the \Kettering Bug" manufactured by General Motors. Both projects were cancelled and the funding stopped as they proved unsuccessful. This is due to the fact of the absence of the required technological advances in the fields of guidance systems and engines (3).

Development of UAVs started increasing tremendously by the end of the 1950s, the USA deployed them during the Vietnam War to decrease the casualties in pilots when flying over hostile territories. After their success, the USA and Israel decided to invest more to build smaller and cheaper UAVs, they used small motors like those found in motorcycles to result in smaller sized and lighter UAVs. In addition, a video camera was added on the UAVs to transmit images to the ground operator. In 1991, the USA used UAVs extensively in the Gulf War, and the most famous model was the Predator shown in Figure I-2. UAVs were intensively used by the USA in many conicts and wars in the late 1990's and early 2000's and later on, UAVs were used extensively in the war against Iraq (4).

Figure I-2:PredatorMilitaryUAV (2)

I.2.1.2 CIVIL HISTORY

The uses of UAVs were not only confined to military use; in 1969, NASA grew a concern to automatically control an aircraft, the first trials was the PA-30 program. The program was successful but they had a pilot onboard to take over the control of the aircraft in case anything went wrong. Other research programs followed the success of the PA-30 program like: Drones for Aerodynamic and Structural Testing (DAST) and Highly Maneuverable Aircraft Technology (HiMAT) programs (5). Following that era, in the 1990's NASA then partnered with industrial companies to develop a nine-year long research project called the Environmental Research Aircraft and Sensor Technology Project (ERAST). They developed several UAVs models that were able to y for altitudes up to 30 Km and endured flights up to 6 months. The resulting UAV models included the: Pathfinder, Helios, Atlus and Perseus B. The developed UAVs carried several sensors to carry out environmental measurements, the onboard sensors included a camera, a Digital Array Scanned Interferometer (DASI) and an active detect, see and avoid (DSA) system (5).

I.2.2 APPLICATIONS OF UAVS

In addition to the military use, UAVs can be used in many civil or commercial applications that are too dull, too dirty or too dangerous for manned aircrafts. These uses include but not limited to:

Earth Science observations from UAVs can be used side-to-side with that acquired from satellites. Such missions include (5):

(a) Measuring deformations in the Earth's crust that may be indications to natural disasters like earthquakes, landslides or volcanos (5).

(b) Cloud and Aerosol Measurements (5).

(c) Tropospheric pollution and air quality measurements to determine the pollution sources and how plumes of pollution are transported from one place to another (5).

(d) Ice sheet thickness and surface deformation for studying global warming (5).

(e) Gravitational acceleration measurements, since the gravitational acceleration varies near Earth, UAVs are used to accurately measure gravitational acceleration at multiple places to define correct references (5).

(f) River discharge is measured from the volume of water owing in a river at multiple points. This will help in global and regional water balance studies (5).

Search and rescue UAVs equipped with cameras are used to search for survivors after natural disasters like earthquakes and hurricanes or survivors from shipwrecks and aircraft crashes .

Wild fire suppression UAVs equipped with infrared sensors are sent to fly over forests prone to fires in order to detect it in time and send a warning back to the ground station with the exact location of the fire before it spreads (5).

Law enforcement UAVs are used as a cost efficient replacement of the traditional manned police helicopters.

Border surveillance UAVs are used to patrol borders for any intruders, illegal immigrants or drug and weapon smuggling (5).

Research UAVs are also used in research conducted in universities to proof certain theories. Also, UAVs equipped with appropriate sensors are used by environmental research institutions to monitor certain environmental phenomena like pollution over large cities.

Industrial applications UAVs are used in various industrial applications such as pipeline inspection or surveillance and nuclear factories surveillance.

Agriculture development UAVs also have agriculture uses such as crops spraying.

I.2.3 CLASSIFICATION OF UAVS

There are different ways to classify UAVs, either according to their range of action aerodynamic configuration, size and payload or according to their levels of autonomy.

I.2.3.1 RANGE OF ACTION CLASSIFICATION

UAVs can be classified into 7 different categories based on their maximum altitude and endurance as follows (6):

(a) High-Altitude Long-Endurance (HALE): they can y over 15000 m high with an endurance of more than 24 hr. They are mainly used for long-range surveillance missions.

(b) Medium-Altitude Long-Endurance (MALE): they can y between 5000- 15000 m of altitude for a maximum of 24 hr. MALE UAVs are also used for surveillance missions.

(c) Medium-Range or Tactical UAV (TUAV): They can y between 100 and 300 km of altitude. They are smaller and operated with simpler systems that their HALE and MALE counterparts.

(d) Close Range UAV: They have an operation range of 100 km. They are mainly used in the civil application such as powerline inspection, crop-spraying, traffic monitoring, homeland security, etc..

(e) Mini UAV (MUAV): They have a weight of about 20 kg and an operating range of about 30 km.

(f) Micro UAV (MAV): They have a maximum wingspan of 150 mm. They are mainly used indoors where they are required to y slowly and hover

(g) Nano Air Vehicles (NAV): They have a small size of about 10 mm. they are mainly used in swarms for applications such as radar confusion. They are also used for short range surveillance if equipped with an equally small camera.

I.2.3.2 AERODYNAMIC CONFIGURATION CLASSIFICATION

UAVs can be classified into four main categories based on their aerodynamic configuration as follows (6):

(a) Fixed-wing UAVs: require a run-way to take-off and land. They can y for a long time and at high cruising speeds. They are mainly used in scientific applications such as meteorological reconnaissance and environmental monitoring, shown in Figure I-3.

Figure I-3:Fixed-Wing UAVs(2)

(a) Single Rotor

(b) Coaxial

(c) Quadrotor

(d) Multi-Rotor

Figure I-4: Rotary-Wing UAVs(1)

(b) Rotary-wing UAVs: they can take off and land vertically. They can also hover and y with high maneuverability. The Rotary-wing UAVs can be further classified into four groups (1):

(i) Single-rotor: they have a main rotor on top and another rotor at the tail for stability, same like the helicopter configuration. Shown in Figure I-4(a).

(ii) Coaxial: they have two rotors rotating in opposite directions mounted to the same shaft. Shown in Figure I-4(b).

(iii) Quadrotor: they have four rotors fitted in a cross-like configuration. Shown in Figure I-4(c).

(iv) Multi-rotor: UAVs with six or eight rotors. They are agile type and y even when a motor fails, as there is redundancy due to the large number of rotors. Shown in Figure I-4(d).

Increasing the number of rotors in turn increases the payload and maximum altitude of the UAVs but it comes at the cost of increasing the size and power consumption.

(c) Blimps UAVs: which may look like balloons or airships, they ensure lifting by their helium-filled body. They are very light and have a large size. They can fly for a long time and at low speeds, shown in Figure I-5.

(d) Flapping-wing UAVs: they are inspired from birds and flying insects. These UAVs have small wings and have an extremely low payload and endurance. On the other hand, they have low power consumption and can perform vertical takeoff and landing. This class of UAVs is still under development, shown in Figure I-6 (2).

Figure I-5:BlimpsUAVs(2)

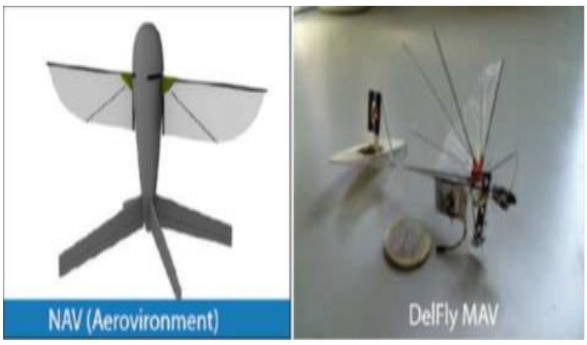

Figure I-6:Flapping Wing UAVs(2)

I.2.3.3 SIZE AND PAYLOAD CLASSIFICATION

UAVs can be classified into five main classes based on their size and payload. Figure I-7 shows examples of these five classes as described below (7):

(a) Full-Scale UAVs: these are normal sized vehicles, shown in Figure I-7(a). Although a pilot can be present on board, the vehicle is capable of autonomousflying. The purpose of the pilot is to backup when trying complex flight tests and maneuvers. Also, these vehicles have the highest payload and endurance.

(b) Medium-scale UAVs: these are the vehicles mainly used for security missions. They have a relatively high payload of 10 kg enabling having heavy and high quality navigation sensors on board, thus achieving dependantflights. Figure I-7(b) shows an example of the Medium Scale UAV used in the US army.

(c) Small-scale UAVs: these are mainly UAVs based on Radio Controlled (RC) toys, they have a lower payload of the range 2 to 10 kg, which enables them to carry adequate quality navigation sensors. An example of a small-scale UAV is shown in Figure I-7(c).

(d) Mini UAVs: portable UAVs that are able to y indoors and outdoors with a payload of less than 2 kg which is sufficient to carry small lightweight sensors. The small size, low cost and ease of maintenance of these UAVs makes them the most common test- bed UAVs in research applications. An example of a mini UAV is shown in Figure I-7(d).

(e) Micro UAVs: mainly used indoors due to their very small size. They have a payload of less than 100 g which makes it very hard to be equipped with navigation and guidance sensors. The research challenge regarding these micro UAVs is to design light-weight navigation and guidance sensors. An example of a micro UAV is shown in Figure I-7(e).

(a) Full-Scale UAV

(b) Medium-ScaleUAVs

(c) Small-ScaleUAVs

(d) Mini UAV

(e) Micro UAV

Figure I-7: Size Classification (7)

I.2.3.4 LEVELS OF AUTONOMY CLASSIFICATION

UAVs can be also classified according to their level of autonomy. The National Institute of Standards and Technology published a framework that can be used to classify UAVs according to their autonomy level which is defined by three metrics namely: Human Independence (HI), Mission Complexity (MC) and Environmental Complexity (EC) [1, 7]. The framework proposes five levels of autonomy [1] shown in figure I-8:

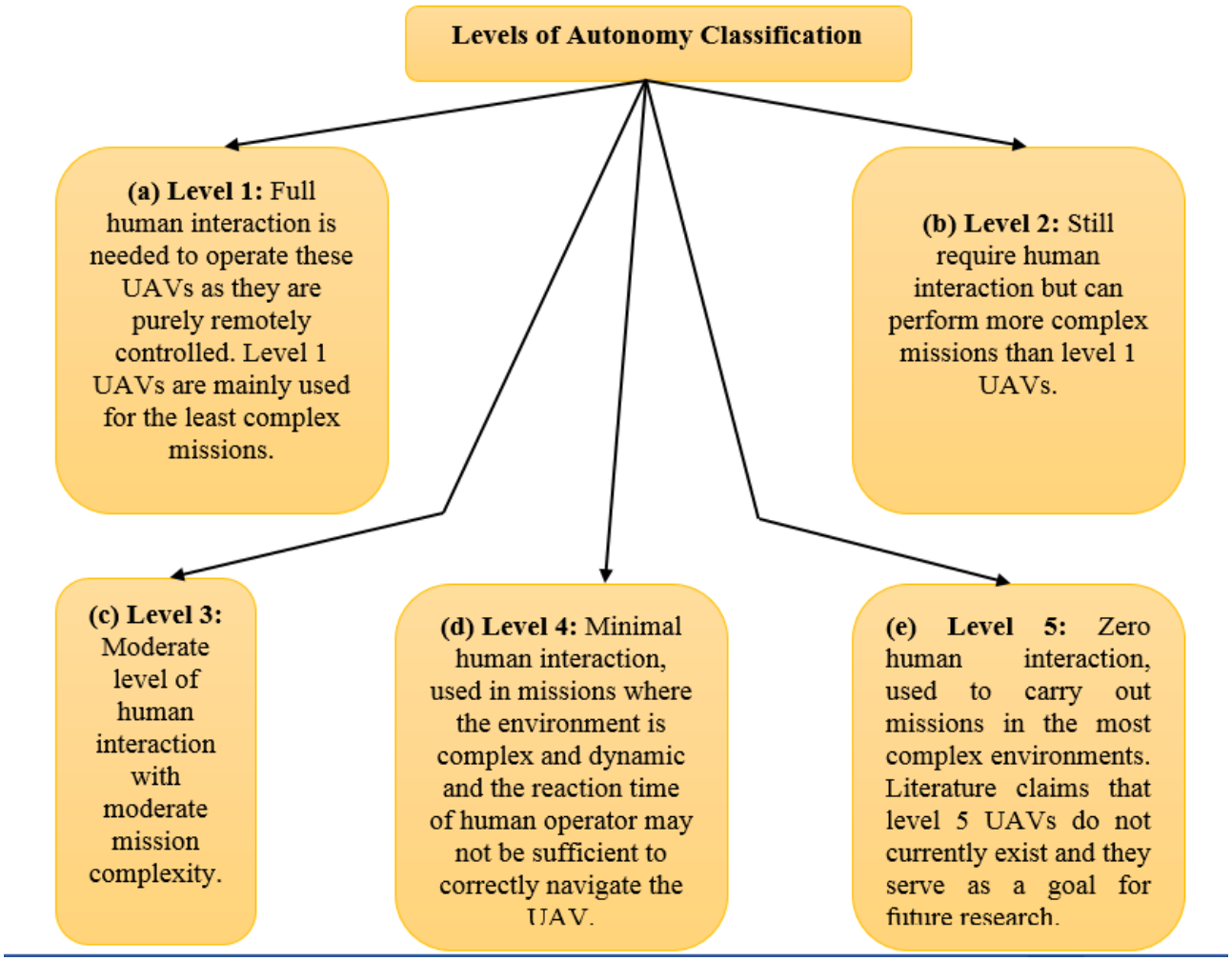

Figure I-8: levels of autonomy classification

I.3 QUADROTORS

The quadrotor concept for aerial vehicles was developed a long time ago. It was reported that the Breguet-Richet quadrotor built in 1907 had actually own. A quadrotor is considered to be a rotary-wing UAV due to its configuration that will be discussed later.

I.3.1 THE QUADROTOR CONCEPT

A quadrotor consists of four rotors, each fitted in one end of a cross-like structure as shown in Figure I-9. Each rotor consists of a propeller fitted to a separately powered DC motor. Propellers 1 and 3 rotate in the same direction while propellers 2 and 4 rotate in an opposite direction leading to balancing the total system torque and cancelling the gyroscopic and aerodynamics torques in stationary flights (8).

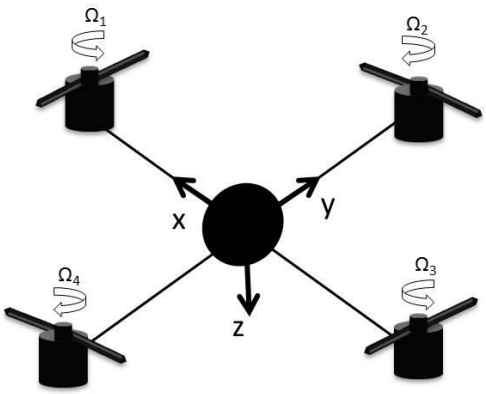

Figure I-9:Quadrotor Configuration(8)

The quadrotor is a 6 DOF object, thus 6 variables are used to express its position in space (x, y, z, ϕ, Θ and ψ). x, y and z represent the distances of the quadrotor's center of mass along the x,y and z axes respectively from an Earth fixed inertial frame. ϕ, Θ and ψ are the three Euler angles representing the orientation of the quadrotor. ϕis called the roll angle which is the angle about the x-axis, Θ is the pitch angle about the y-axis, while is the yaw angle about the z-axis. Figure I-10 clearly explains the Euler Angles. The roll and pitch angles are usually called the attitude of the quadrotor, while the yaw angle is referred to as the heading of the quadrotor. For the linear motion, the distance from the ground is referred to as the altitude and the x and y position in space is often called the position of the quadrotor.

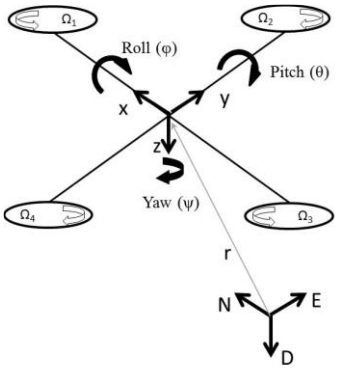

Figure I-10: Euler Angles for a Quadrotor UAV(8)

To generate vertical upwards motion, the speed of the four propellers is increased together whereas the speed is decreased to generate vertical downwards motion. To produce roll rotation coupled with motion along the y-axis, the second and fourth propellers speeds are changed while for the pitch rotation coupled with motion alongthe x-axis, it is the _rst and third propellers speeds that need to be changed.

One problem with the quadrotor configuration is that to produce yaw rotation, one need to have a difference in the opposite torque produced by each propeller pair.

For instance, for a positive yaw rotation, the speed of the two clockwise turning rotors need to be increased while the speed of the two counterclockwise turning rotors need to be decreased. Figure I-11 shows how different movements can be produced, note that a thicker arrow means a higher propeller speed.

I.3.2 ADVANTAGES AND DRAWBACKS OF QUADROTORS

Some advantages of the quadrotor over helicopters is that the rotor mechanics are simplified as it depends on four fixed pitch rotors unlike the variable pitch rotor in the helicopter, thus leading to easier manufacturing and maintenance. Moreover, due to the symmetry in the configuration, the gyroscopic effects are reduced leading to simpler control.

Stationary hovering can be more stable in quadrotors than in helicopters due to the presence of four propellers providing four thrust forces shifted a fixed distance from the center of gravity instead of only one propeller centered in the middle as in the helicopters structure.

More advantages are the vertical take-off and landing capabilities, better maneuverability and smaller size due to the absence of a tail, these capabilities make quadrotors useful in small area monitoring and buildings exploration.

Moreover, quadrotors have higher payload capacities due to the presence of four motors thus providing higher thrust.

On the other hand, quadrotors consume a lot of energy due to the presence of four separate propellers .Also, they have a large size and heavier than some of their counterparts again to the fact that there is four separate propellers (9).

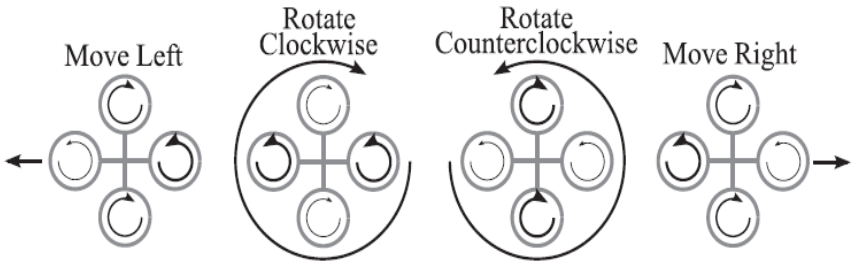

Figure I-11: Generated Motion of the Quadrotor (9)

I.4 FORMATION OF QUADROTORS

In some cases, a single UAV cannot well perform some complex missions, such as large payloads transportation, searching objects in large area, etc. Motivated by these potential applications, researchers are more and more attracted by the cooperation of multiple UAVs.

The quadrotors have a fundamental payload limitation that is difficult to over-come in many practical applications, especially in large payloads transportations. GRASP laboratory at University of Pennsylvania has investigated the payload limitations of micro aerial robots and they proposed to manipulate and transport the large payloads by multiple UAVs (10)(11), which are shown in Fig.I.13.Within the project of ”Flying Machine Arena” at ETH Zurich, the researchers carry out a flexible payload transportation task using the cooperation of multiple quadrotors (12)which is shown in Fig.I-12(a). In the same laboratory, the cooperative quadrotors are also used for architecture (see Fig.I-12(b)). In these works, the cooperation of quadrotors are achieved under the help of a localization system.

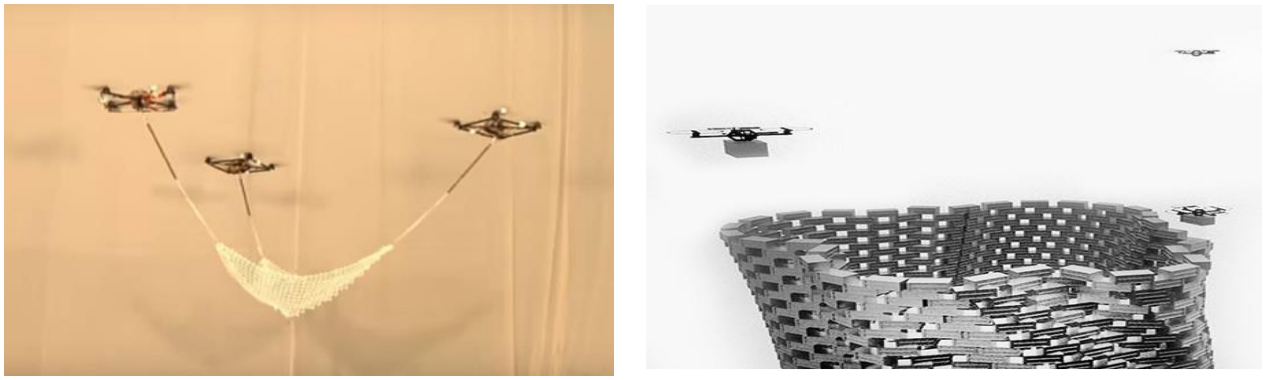

(a) Flexible payload (b) Architecture

FigureI-12: Cooperation of multiple quadrotors(12)

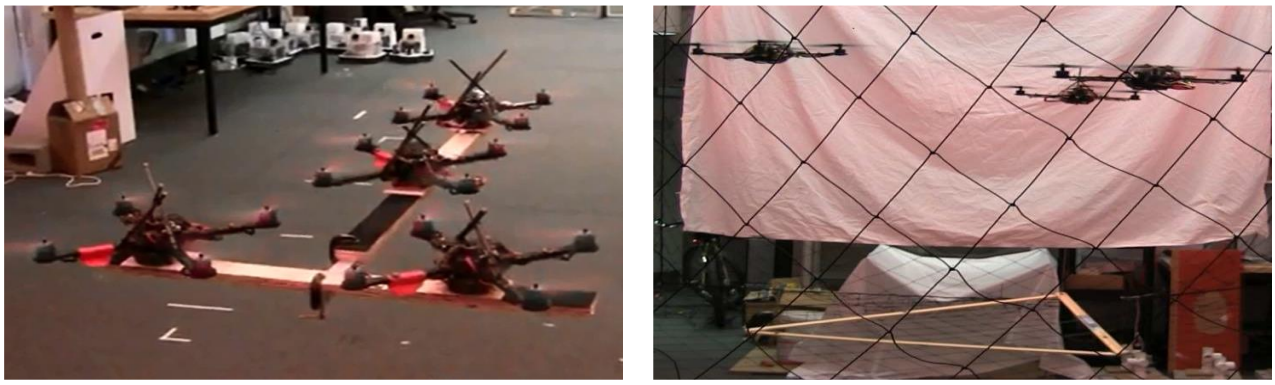

Figure I-13 : Large objects transportation by using multiple quadrotors(12)

Some applications such as surveillance and searching objects require the cooperation of quadrotors in outdoor environment. As shown in Fig.I-14, the task of cooperative surveillance in large outdoor areas by a fleet of micro aerial vehicles is proposed in (13). At Czech Technical University, the localization of quadrotors in outdoor environment are proposed by using an efficient vision-based method.

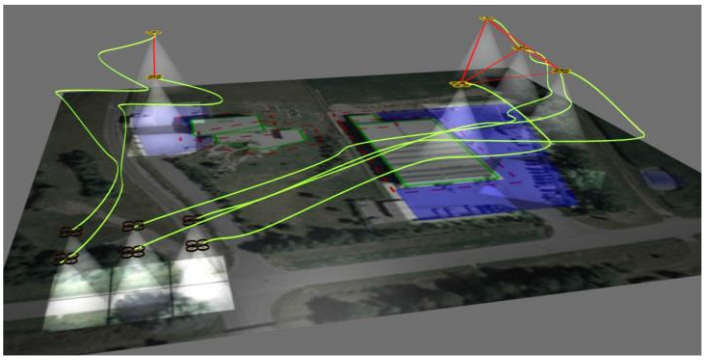

Figure I-14: Group of quadrotors deployed in the environment to cover the areas of interest by on-board surveillance cameras (13).

I.4.1 REPRESENTATION OF A QUADROTORS FORMATION

I.4.1.1 MULTI-AGENT SYSTEM (MAS)

The natural behavior of animals operating as a team has inspired scientists in different disciplines to investigate the possibilities of networking a group of systems to accomplish a given set of tasks without requiring an explicit supervisor. Therefore, multi-agent systems have appeared broadly in several applications including multi-vehicle system, formation flight of unmanned air vehicles (UAVs), clusters of satellites, self-organization, automated high way systems, and congestion control in communication networks. A formation of multiple quadrotors can be modeled

as a multi-agent system. The methodology in multi-agent system can be used for reference in the study of multi-quadrotor formation problem.

I.4.1.2 SYSTEMS OF SYSTEMS (SOS)

Systems of Systems (SoSs) are large-scale integrated systems which are heterogeneous and independently operable on their own, but are networked together for a common goal . These systems could be robotic, automatic or Even human (14). The Autonomous Control Engineering (ACE) lab at the University of Texas is trying to take systems of different types of robots to build systems of systems, see Fig.1-15 for example.

Figure I-15: Examples of modern application of SoS(14).

This thesis is organized as follows :

Chapter 2: presents the mathematical modeling of a quadrotor UAV based on the Newton-Euler formalism in full details including the DC Motors and aerodynamic effects acting on the quadrotor body. Besides that a control alogorithm is devlopped to stabilize the quadrotor movements, this controller is going to be implemented on MATLAB/Simulink to asses its performance.

Chapter 3: discusses the path planning and obstacle avoidane for a single quadrotor using a specific algorithm.

Chapter 4: shows the formation control strategies for the multi-quadrotors system. And in the end a general conclusion for this work is given at the end of the general introduction .

II. CHAPTER : QUADROTOR MODELING & CONTROL

II.1 INTRODUCTION

In this chapter, the derivation of the quadrotor model is provided. This result is very important because it describes how the helicopter moves according to its inputs. Thanks to these equations it is possible to define and predict the positions reached by the helicopter by investigating just the four motor speeds. Then a flight control algorithm will be designed for the quadrotor based on the mathematical model developed earlier, The PID controller was chosen as the control technique to stabilize (control attitude) the quadrotor model in flight.

After deriving the kinematics and dynamics models of the quadrotor, the aerodynamic effects acting on the quadrotor body will be discussed together with the rotor dynamics of the actuators of the quadrotor. The chapter will be ended with formulating a state space model for the quadrotor system that will be used in the subsequent modeling chapter.

II.2 KINEMATIC MODEL

The kinematics and dynamics models of a quadrotor will be derived based on a Newton-Euler formalism with the following assumptions:

- ✓ The structure is rigid and symmetrical.
- ✓ The center of gravity of the quadrotor coincides with the body fixed frame origin.
- ✓ The propellers are rigid.
- ✓ Thrust and drag are proportional to the square of propeller's speed.

In order to discuss the modeling of the quadrotor, we first need to define the coordinate frames that will be used. Figure II-1 shows the Earth reference frame with N, E and D axes and the body frame with x, y and z axes. The Earth frame is an inertial frame fixed on a specific place at ground level as its name implies, it uses the N-E-D notation where the axes point to the North, East and Downwards respectively. On the other hand, the body frame is at the center of the quadrotor body, with its x-axis pointing towards propeller 1, y-axis pointing towards propeller 2 and the z-axis is pointing to the ground.

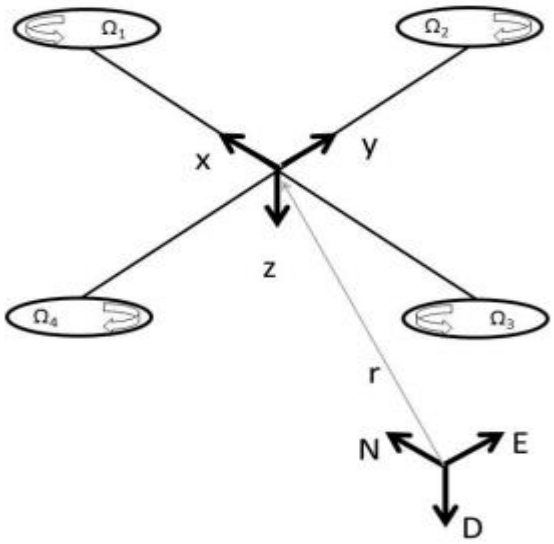

Figure II-1:Quadrotor Reference Frames

The distance between the Earth frame and the body frame describes the absolute position of the center of mass of the quadrotor$r = [xyz]^T$. The rotation R from the body frame to the inertial frame describes the orientation of the quadrotor. The orientation of the quadrotor is described using roll, pitch and yaw angles (φ, θ and ψ) representing rotations about the X, Y and Z-axes respectively. Assuming the order of rotation to be roll (φ), pitch (θ) then yaw (ψ), the rotation matrix R which is derived based on the sequence of principle rotations is:

$$R = \begin{bmatrix} c\theta c\psi & s\phi s\theta c\psi & c\phi s\theta c\psi + s\phi s\psi \\ c\theta s\psi & s\phi s\theta s\psi + c\theta c\psi & c\phi s\theta s\psi - s\theta c\psi \\ -s\theta & s\phi c\theta & c\phi c\theta \end{bmatrix} \quad \text{(II.1)}$$

where$c$ and s denote cos andsin respectively. The derivation of the rotation matrix $R$is shown in details in Appendix A.1.1.

The rotation matrix R will be used in formulating the dynamics model of the quadrotor, its significance is due to the fact that some states are measured in the body frame (e.g. the thrust forces produced by the propellers) while some others are measured in the inertial frame (e.g. the gravitational forces and the quadrotor's position). Thus, to have a relation between both types of states, a transformation from one frame to the other is needed.

To acquire information about the angular velocity of the quadrotor, typically an on-board Inertial Measurement Unit (IMU) is used which will in turn give the velocity in the body coordinate frame. To relate the Euler rates $\dot{\eta} = \left[\dot{\phi}\dot{\theta}\dot{\psi}\right]^T$ that are measured in the inertial frame and angular body rates$\omega = [pqr]^T$, a transformation is needed as follows:

$$\omega = R_r \dot{\eta} \tag{II.2}$$

Where

$$R_r = \begin{bmatrix} 1 & 0 & -sin\theta \\ 0 & cos\phi & sin\phi cos\theta \\ 0 & -sin\phi & cos\phi cos\theta \end{bmatrix}$$

Around the hover position, small angle assumption is made where$cos\phi \equiv 1$,$cos\theta \equiv 1$and $sin\phi = sin\theta = 0$. Thus $R_r$can be simplified to an identity matrix I[33]. The derivation for the previous transformation is shown in Appendix A.1.2.

II.3 DYNAMICS MODEL

The motion of the quadrotor can be divided into two subsystems; rotational subsystem (roll, pitch and yaw) and translational subsystem (altitude and x and y position).

The rotational subsystem is fully actuated while the translational subsystem is underactuated(15).

II.3.1 ROTATIONAL EQUATIONS OF MOTION

The rotational equations of motion are derived in the body frame using the Newton Euler method with the following general formalism,

$$J\dot{\omega} + \omega \times J\omega + M_G = M_B \tag{II.3}$$

Where:

J : Quadrotor's diagonal inertia Matrix

ω : Angular body rates

M_G : Gyroscopic moments due to rotors' inertia

M_B : Moments acting on the quadrotor in the body frame

The first two terms of Equation II.3, $J\dot{\omega}$and$\omega \times J\omega$, represent the rate of change of angular momentum in the body frame. While $M_G$represent the gyroscopic moments due to the rotors' inertia J_r. The Gyroscopic momentsare defined to be$\omega \times [0\ 0\ J_r\Omega_r]^T$, thus the rotational equation of the quadrotor's motion can be written as,

$$J\dot{\omega} + \omega \times J\omega + \omega \times [0\ 0\ J_r\Omega_r]^T = M_B \quad \text{(II.4)}$$

Where:

J_r : rotors' inertia

Ω_r : rotors' relative speed

$$\Omega_r = -\Omega_1 + \Omega_2 - \Omega_3 + \Omega_4$$

The reason behind deriving the rotational equations of motion in the body frame and not in the inertial frame is to have the inertia matrix independent on time.

II.3.1.1 INERTIA MATRIX

The inertia matrix for the quadrotor is a diagonal matrix, the off-diagonal elements, which are the product of inertia, are zero due to the symmetry of the quadrotor.

$$J = \begin{bmatrix} I_{xx} & 0 & 0 \\ 0 & I_{yy} & 0 \\ 0 & 0 & I_{zz} \end{bmatrix} \quad \text{(II.5)}$$

Where I_{xx}, I_{yy} and I_{zz} are the area moments of inertia about the principle axes in the body frame.

II.3.1.2 GYROSCOPIC MOMENT

The gyroscopic moment of a rotor is a physical effect in which gyroscopic torques or moments attempt to align the spin axis of the rotor along the inertial z-axis (16).

II.3.1.3 MOMENTS ACTING ON THE QUADROTOR (M_B)

For the last term of equation (II.4), there is a need to define two physical effects, which are the aerodynamic forces and moments produced by a rotor. As an effect of rotation, there is a generated force called the aerodynamic force or the lift force and there is a generated moment called the aerodynamic moment. Equations (II.6) and (II.7) show the aerodynamic force F_i and moment M_i produced by the i^{th} rotor (2).

$$F_i = \frac{1}{2}\rho A\, C_T r^2 \Omega_i^2 \quad \text{(II.6)}$$

$$M_i = \frac{1}{2}\rho A\, C_D r^2 \Omega_i^2$$

(II.7)

Where:

ρ : Air density

A : Blade area

C_T , C_D : aerodynamic coefficients

r_b : Radius of blade

Ω_i : Angular velocity of rotor i

Clearly, the aerodynamic forces and moments depend on the geometry of the propeller and the air density. Since for the case of quadrotors, the maximum altitude is usually limited thus the air density can be considered constant, Equations (II.6) and (II.7) can be simplified to (15),

$$F_i = K_f \Omega_i^2 \quad \text{(II.8)}$$

$$M_i = K_M \Omega_i^2 \quad \text{(II.9)}$$

Where K_f and K_M are the aerodynamic force and moment constants respectively and Ω_i is the angular velocity of rotor i. The aerodynamic force and moment constants can be determined experimentally for each propeller type.

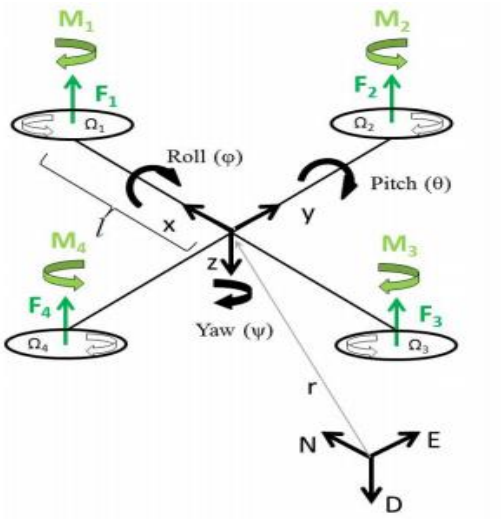

Figure II-2: Forces and Moments acting on Quadrotor(15)

By identifying the forces and moments generated by the propellers, we can study the moments

M_B acting on the quadrotor. Figure II-2 shows the forces and moments acting on the quadrotor. Each rotor causes an upwards thrust force F_i and generates a moment M_i with direction opposite to

The direction of rotation of the corresponding rotor i.

Starting with the moments about the body frame's x-axis, by using the right-hand-rule in association with the axes of the body frame, F_2 multiplied by the moment arm l generates a negative moment about the y-axis, while in the same manner, F_4generates a positive moment. Thus the total moment about the x-axis can be expressed as,

$$\begin{aligned} M_x &= -F_2 l + F_4 l \\ &= -K_f \Omega_2^2 l + K_f \Omega_4^2 l \\ &= l K_f (-\Omega_2^2 + \Omega_4^2) \end{aligned} \tag{II.10}$$

For the moments about the body frame's y-axis, also using the right-hand-rule, the thrust of rotor 1 generates a positive moment, while the thrust of rotor 3 generates a negative moment about the y-axis. The total moment canbeexpressed as,

$$\begin{aligned} M_y &= -F_1 l + F_3 l \\ &= -K_f \Omega_1^2 l + K_f \Omega_3^2 l \end{aligned} \tag{II.11}$$

$$= lK_f(-\Omega_1^2 + \Omega_3^2)$$

For the moments about the body frame's z-axis, the thrust of the rotors does not cause a moment. On the other hand, moment caused by the rotors' rotation as per equation II.7. By using the right-hand-rule, the moment about the body frame's z-axis can be expressed as,

$$\begin{aligned} M_z &= M_1 - M_2 + M_3 - M_4 \\ &= (K_M\Omega_1^2) - (K_M\Omega_2^2) + (K_M\Omega_3^2) - (K_M\Omega_4^2) \\ &= K_M(\Omega_1^2 - \Omega_2^2 + \Omega_3^2 - \Omega_4^2) \end{aligned} \quad \text{(II.12)}$$

Combining equations (II.10), (II.11) and (II.12) in vector form, we get,

$$M_B = \begin{bmatrix} lK_f\left(-\Omega_2^2 + \Omega_4^2\right) \\ lK_f\left(-\Omega_1^2 + \Omega_3^2\right) \\ K_M\left(\Omega_1^2 - \Omega_2^2 + \Omega_3^2 - \Omega_4^2\right) \end{bmatrix} \quad \text{(II.13)}$$

Where$l$ is the moment arm, which is the distance between the axis of rotation of each rotor to the origin of the body reference frame which should coincide with the center of the quadrotor.

II.3.2 TRANSLATIONAL EQUATIONS OF MOTION

The translation equations of motion for the quadrotor are based on Newton's second law and they are derived in the Earth inertial frame (15),

$$m\ddot{r} = \begin{bmatrix} 0 \\ 0 \\ mg \end{bmatrix} + RF_B \quad \text{(II.14)}$$

Where

$r = [xyz]^T$ Quadrotor's distance from the inertial frame

m : Quadrotor's mass

g : gravitational acceleration $g = 9.81m/s^2$

F_B : nongravitational forces acting on the quadrotor in the body frame

II.3.2.1 NONGRAVITATIONAL FORCES ACTING ON THE QUADROTOR

When the quadrotor is in a horizontal orientation (i.e. it is not rolling or pitching), the only nongravitational forces acting on it is the thrust produced by the rotation of the propellers which is proportional to the square of the angular velocity of the propeller as per Equation (II.8). Thus, the nongravitational forces acting on the quadrotor, F_B, can be expressed as,

$$F_B = \begin{bmatrix} 0 \\ 0 \\ -K_f\left(\Omega_1^2 + \Omega_2^2 + \Omega_3^2 + \Omega_4^2\right) \end{bmatrix} \quad \text{(II.15)}$$

The first two rows of the force vector are zeros as there is no forces in the X and$Y$ directions, the last row is simply an addition of the thrust forces produced by the four propellers. The negative sign is due to the fact that the thrust is upwards while the positive z-axis in the body framed is pointing downwards.

$F_B$is multiplied by the rotation matrix R to transform the thrust forces of the rotors from the body frame to the inertial frame, so that the equation can be applied in any orientation of the quadrotor.

II.4 AERODYNAMIC EFFECTS

In the previous dynamics formulation, the aerodynamic effects acting on the quadrotor body were neglected. However, in order to have an accurate and realistic model to be used in simulations, aerodynamic effects should be included. There are namely two types of aerodynamic effects, drag forces and drag moments(17).

II.4.1 DRAG FORCES

Due to the friction of the moving quadrotor body with air, a force acts on the body of the quadrotor resisting the motion. As the velocity of travel of the quadrotor increases, the drag forces in turn increase. The drag forces F_a can be approximated by,

$$F_a = K_t\dot{r} \quad \text{(II.16)}$$

whereK_t is a constant matrix called the aerodynamic translation coefficient matrix and $\dot{r}$ is the time derivative of the position vector r. This indicates that there is an extra force acting on the quadrotor body, the translational equation of motion Equation (II.14) should be rewritten to be,

$$m\ddot{r} = \begin{bmatrix} 0 \\ 0 \\ mg \end{bmatrix} + RF_B - F_a \quad \text{(II.17)}$$

II.4.2 DRAG MOMENTS

The same as the drag force, due to the air friction, there is a drag moment M_a acting on the quadrotor body which can be approximated by,

$$M_a = K_r\dot{\eta} \quad \text{(II.18)}$$

WhereK_r is a constant matrix called the aerodynamic rotation coefficient matrix and $\dot{\eta}$ is the Euler rates. Accordingly, the rotational equation of motion expressed by Equation (II.4) can be rewritten to as,

$$J\dot{\omega} + \omega \times J\omega + \omega \times [0\ 0\ J_r\Omega_r]^T = M_B - M_a \quad \text{(II.19)}$$

II.5 DC BRUSHLESS MOTOR

The DC-motor is an actuator which converts electrical energy into mechanical energy (and vice versa). It is composed of two interactive electromagnetic circuits. The first one (called rotor) is free to rotate around the second one (called stator) which is fixed instead. In the rotor, several groups of copper windings are connected in series and are externally accessible thanks to a device called

commutator. In the stator, two or more permanent magnets impose a magnetic field which affects the rotor. By applying a DC-current flow into the windings, the rotor turns because of the force generated by the electrical and magnetic interaction. Thanks to the rotor and the commutator geometries, the motor keeps turning while supplied by a DC-voltage on its terminals. These are just a few basic concepts to understand the following section.

The DC-motor has a well known model which binds electrical and mechanical quantities. This model is composed of the series of a resistor R [Ω] , an inductor L [H] and a voltage generator e [V]. The resistor represents the Joule loss due to the current flow into the copper conductor. Its value depends on geometric and material characteristics such as wire resistivity, length and section. The inductor behavior derives from the shape of the motor wires which are winded in the middle of the

rotor. Lastly, the generator e (called also BEMF) supplies a voltage proportional to the motor speed. The model isrepresented in figure II-3.(8)

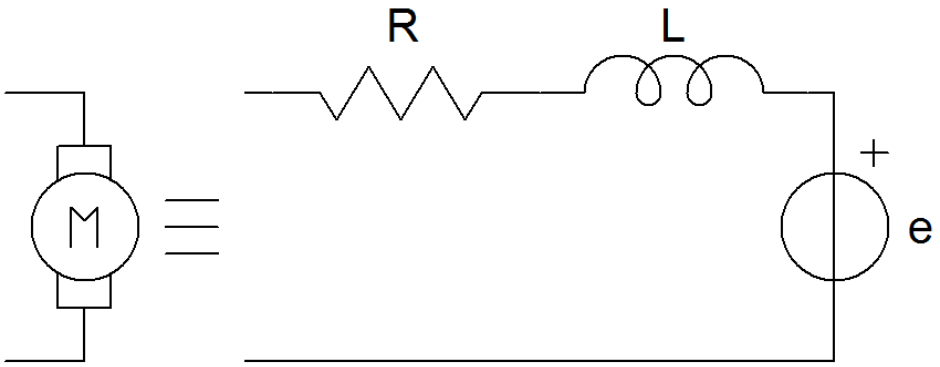

Figure II-3:Motor model(8)

The circuit of the DC-motor is controlled by a real voltage generator v[V]which gives the control input. In theory, another resistor should be added in series of the voltage generator representing the driver losses. However, in a good project, the generator losses are kept low therefore it is possible to neglect them in the model. The basic electrical circuit isshown in figure II-4.

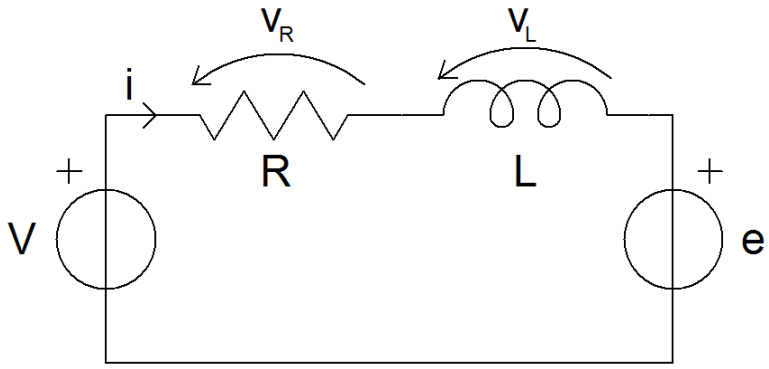

Figure II-4:Motor circuit

By applying the Kirchhoff's voltage law, it follows equation (II.20).

$$v = v_R + v_L + e \tag{II.20}$$

Where v_R [V] is the voltage across the resistor R and v_L [V] is the voltageacross the inductor L. Equation (II.21) can be rewritten as in the next equation.

$$v = Ri + L\frac{di}{dt} + K_E\omega_M \tag{II.21}$$

i [A] is the motor current, K_E [V s rad^{-1}] is called the motor constant andω_M [rad s^{-1}] is the motor angular speed. The first addend has been changed using the Ohm's law v_R= Ri, while the second

one using the inductor differential equation $v_L = L\frac{di}{dt}$. The last member of equation (II.21) shows that mechanics and electricsare correlated.

The contribution of the inductor part is important to determine the characteristic of the DC-motor driver. However is often neglected in the mechanics computation because of three main aspects:

• Most of the motors used in robotics show small inductance thanks to construction optimization.

• The pole (response time) of the electrical part is always much faster than the mechanic one, therefore the speed of the overall system will be determined just by the slowest contribution.

• It's much easier to solve a first order differential equation rather than a second order one.

For all these reasons the inductor effect was neglected in this work too. Thereforeequation (II.21) canbesimplifiedaccording to equation (II.22).

$$v = Ri + K_E\omega_M \tag{II.22}$$

The dynamics of the motor is described by the following equation.

$$J_{TM}\dot{\omega_M} = T_M - T_L \tag{II.23}$$

Where J_{TM} [N m s^2] is the total motor moment of inertia,$\dot{\omega_M}$ [rad s^2] isthe motor angular acceleration, T_M [N m] is the motor torque and T_L [N m] is the load torque. Equation (II.23) states that when the motor torque T_M and the load torque T_L are not equal, there is an acceleration (or deceleration) of the motor angular speedω_M. This variation of speed depends also on the total motor moment of inertiaJ_{TM}: the smaller the value ofJ_{TM}, the higher the acceleration. Figure II-5 shows a sketch of the simplifiedmechanic structure.

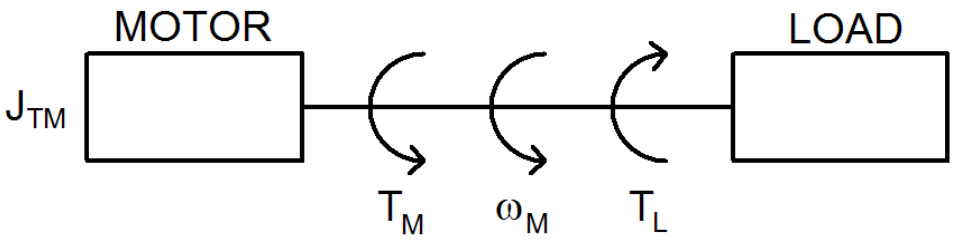

Figure II-5:Simplifiedmotor system(8)

The motor torque T_M is proportional to the electrical current i through K_M [N m A^{-1}]: $T_M = K_M$i. Hence equation (II.23) can be rewritten according to equation (II.24).

$$J_{TM}\dot{\omega}_M = K_M i - T_L \tag{II.24}$$

By connecting equations (II.22) and (II.24) a differential equation in ω_M can be derived.

$$J_{TM}\dot{\omega}_M = \frac{K_E K_M}{R}\omega_M - T_L + \frac{K_M}{R}v \tag{II.25}$$

It must be pointed out that the two constants K_E and K_M have the same value even though the units of measurement differ. This mismatch comes from the electric P_E [W] and mechanic P_M [N m s^{-1}] power balance.

$$P_E = P_M \begin{Bmatrix} P_E = ei = K_E i\omega_M \\ P_M = T_M\omega_M = K_M i\omega_M \end{Bmatrix} \Rightarrow K_E = K_M \tag{II.26}$$

The real motor system is composed of the motor itself, the gear box and the propeller. A few equations must be added to take into account these connections. Figure II-6 shows the structural system.

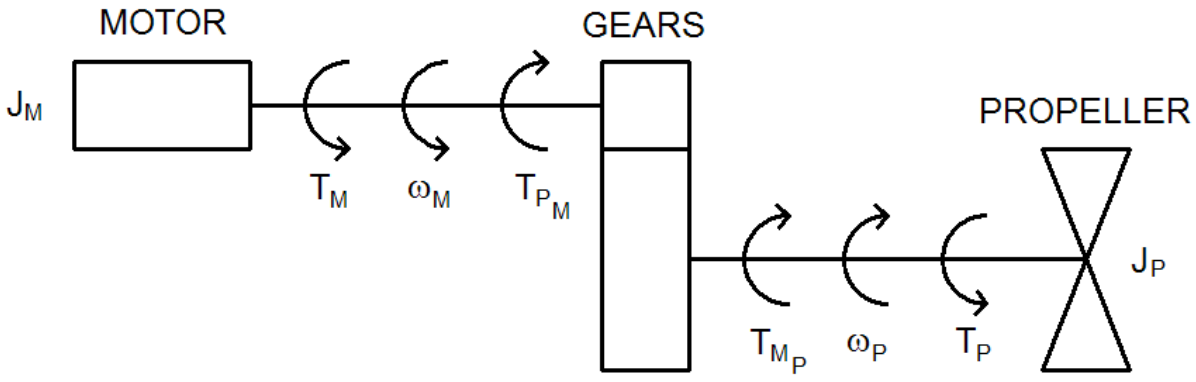

Figure II-6:Motor system(8)

In figure III.9 several variables have been introduced: J_M [N m s^2] is the rotor moment of inertia around the motor axis, J_P [N m s^2] is the rotor moment of inertia around the propeller axis, ω_P [rad s^2] is the propeller angular speed, T_{PM} [N m] is the propeller torque in the motor axis, T_P [N m] is the propeller torque and T_{MP} [N m] is the motor torque in the propeller axis. The gear box has a reduction ratio N [−] equal to the motor speed ω_M divided by the propeller speed ω_P: N = $\frac{\omega_M}{\omega_P}$.

N can be also calculated as the ratio of the number of teeth of the propeller gear to the number of teeth of the motor gear.

Another parameter of the gear box is the conversion efficiency $\eta[-]$ which binds the mechanical power of the motor axis P_M to the propeller axis one P_P [N m s^{-1}].

$$\begin{aligned} P_M\eta &= P_P \\ \omega_M T_{PM}\eta &= \omega_P T_{MP} \end{aligned} \tag{II.27}$$

Therefore, it is possible to calculate the dynamics of the gear box system according to the following steps.

$$J_M\dot{\omega}_M = T_M - T_{PM} \tag{II.28}$$

$$J_P\dot{\omega}_P = T_{MP} - T_P \tag{II.29}$$

Where $\dot{\omega}_P$[rad s^{-2}] is the propeller angular acceleration. Equation (II.38) can be rewritten (taking into account equations (II.28) and (II.29) as follows.

$$\begin{aligned} \omega_M(T_M - J_M\dot{\omega}_M)\eta &= \omega_P(T_P + J_P\dot{\omega}_P) \\ \left(J_M + \frac{J_P}{\eta N^2}\right)\omega_M &= T_M - \frac{T_p}{\eta N} \end{aligned} \tag{II.30}$$

In equation (II.30) the following two substitutions were done.

$$\dot{\omega}_P = \frac{\omega_P}{\omega_M}\dot{\omega}_M \text{ And} \frac{\omega_M}{\omega_P} = N$$

Equation (II.30) is very important because it has the same structure of equation (II.23). Comparing the two equations, the real values of the load torque T_L and the total motor moment of inertia J_{TM} can be derived according to equations (II.31) and (II.32).

$$T_L = \frac{T_p}{\eta N} \tag{II.31}$$

$$J_{TM} = \left(J_M + \frac{J_P}{\eta N^2}\right) \tag{II.32}$$

The parameters in equations (II.31) and (II.32) can be calculated by geometric, dynamic and aerodynamic evaluation of the mechanic structure. Equation (II.33) follows from aerodynamic calculus (for more information see (8)).

$$T_P = d\omega_P^2 = \frac{d\omega_M^2}{N^2} \tag{II.33}$$

Where d [N m s^2] is the aerodynamic drag factor. From equations (II.31) and (II.33) the final load torque expression can be

$$T_L = \frac{d\omega_M^2}{\eta N^3} \tag{II.34}$$

Equations (II.25) can be rewritten according to equations (II.32) and (II.34).

$$\left(J_M + \frac{J_P}{\eta N^2}\right))\dot{\omega_M} = -\frac{K_E K_M}{R}\omega_M - \frac{d\omega_M^2}{\eta N^3} + \frac{K_M}{R}v \tag{II.35}$$

All these previous equations can be reformulated with reference to the propeller axis (and not the motor one). Therefore, the motor system can be also modeled with the following differential equation.

$$\left(J_P + \eta N^2 J_M\right)\dot{\omega_P} = -\frac{K_E K_M}{R}\eta N^2 \omega_P - d\omega_P^2 + \frac{K_M}{R}\eta N v \tag{II.36}$$

Where the $\dot{\omega}_P$ coefficient is the total rotational moment of inertia around the propeller axis (J_{TP} [N m s^2]) as shown in equation (II.37).

$$J_{TP} = J_P + \eta N^2 J_M \tag{II.37}$$

Since the differential equation equation (II.36) is non linear, a good approach is to linearize it around its working point. The first order Taylor series method has been adopted to derive equation (II.38).

$$\dot{\omega}_P = A_P\omega_P + B_P v + C_P \tag{II.38}$$

In the previous equation A_P [rad s^{-1}] is the linearized propeller's speed coefficient, B_P[$rad^2 s^{-2} v^{-1}$] is the linearized input voltage coefficient and C_P [$rad^2 s^{-2}$] is the linearized constant coefficient. Their values are defined according to equations (II.39), (II.40) and (II.41).

$$A_P = \frac{\partial \dot{\omega}_p}{\partial \omega_p} = \frac{-K_E K_M \eta N^2}{J_{TP} R} - \frac{2d}{J_{TP}} \omega_H = -22.5[rad\, s^{-1}] \quad \text{(II.39)}$$

$$C_p = \frac{\partial \dot{\omega}_p}{\partial v} = \frac{K_M \eta N}{J_{TP} R} = 509[rad^2 s^{-2} V^{-1}] \quad \text{(II.40)}$$

$$C_P = \dot{\omega}_P - (A_P \omega_P + B_P v) = \frac{d}{J_{TP}} \omega_H^2 = 482[rad^2 s^{-2}] \quad \text{(II.41)}$$

Therefore, with just these three parameters it is possible to describe the dynamics of all the four motors systems. Equation (II.42) shows the differentialequation in a matrix form.

$$\dot{\Omega} = A_P \Omega + B_P v + C_P \quad \text{(II.42)}$$

Where Ω [rad s^{-1}] is the propellers' speed vector, $\dot{\Omega}$[rad s^{-2}] is the propellers' acceleration vector and v [V] is the inputs' voltage vector.

II.6 STATE SPACE MODEL

Formulating the acquired mathematical model for the quadrotor into a state space model will help make the control problem easier to tackle.

II.6.1 STATE VECTOR X

Defining the state vector of the quadrotor to be,

$$X = [x_1 x_2 x_3\, x_4 x_5 x_6 x_7 x_8\, x_9 x_{10} x_{11} x_{12}]^T \quad \text{(II.43)}$$

which is mapped to the degrees of freedom of the quadrotor in the following manner,

$$X = \left[\phi\ \dot{\phi}\ \theta\ \dot{\theta}\ \psi\ \dot{\psi}\ \ z\ \dot{z}\ x\ \dot{x}\ y\ \dot{y}\right]^T \quad \text{(II.44)}$$

The state vector defines the position of the quadrotor in space and its angular and linear velocities.

II.6.2 CONTROL INPUT VECTOR *U*

A control input vector, U, consisting of four inputs; U_1 through U_4 is defined as,

$$U = [U_1 U_2 U_3 U_4] \quad \text{(II.45)}$$

Where

$$U_1 = K_f \left(\Omega_1^2 + \Omega_2^2 + \Omega_3^2 + \Omega_4^2\right)$$

$$U_2 = K_f \left(-\Omega_2^2 + \Omega_4^2\right)$$

$$U_3 = K_f\left(\Omega_1^2 - \ \Omega_3^2\right) \tag{II.46}$$

$$U_4 = K_M\left(\Omega_1^2 - \ \Omega_2^2 + \ \Omega_3^2 \ - \ \Omega_4^2\right) \tag{II.47}$$

(II.48)

(II.49)

Equations (II.46) through (II.49) can be arranged in a matrix form to result in,

$$\begin{bmatrix} U_1 \\ U_2 \\ U_3 \\ U_4 \end{bmatrix} = \begin{bmatrix} K_f K_f K_f K_f \\ 0 \ -K_f \ 0 \ K_f \\ K_f \ 0 \ -K_f \ 0 \\ K_M \ -K_M K_M \ -K_M \end{bmatrix} \begin{bmatrix} \Omega_1^2 \\ \Omega_2^2 \\ \Omega_3^2 \\ \Omega_4^2 \end{bmatrix} \tag{II.50}$$

$U_1$is the resulting upwards force of the four rotors which is responsible for thealtitude of the quadrotor and its rate of change (z;$\dot{z}$). U_2Is the difference in thrust between rotors 2 and 4 which is responsible for the roll rotation and its rate of change (ϕ; $\dot{\phi}$). U_3On the other hand represents the difference in thrust between rotors 1 and 3 thus generating the pitch rotation and its rate of change (Θ; $\dot{\Theta}$). Finally $U_4$is the difference in torque between the two clockwise turning rotors and the two counterclockwise turning rotors generating the yaw rotation and ultimately its rate of change(ψ; $\dot{\psi}$). This choice of the control vector U decouples the rotational system, whereU_1 will generate the desired altitude of the quadrotor, U_2will generate the desired roll angle, the desired pitch angle will be generated by U_3 whereas U_4will generate the desired heading.

If the rotor velocities are needed to be calculated from the control inputs, an inverse relationship between the control inputs and the rotors' velocities is needed, which can be acquired by inverting the matrix in Equation (II.50) to give,

$$\begin{bmatrix} \Omega_1^2 \\ \Omega_2^2 \\ \Omega_3^2 \\ \Omega_4^2 \end{bmatrix} = \begin{bmatrix} 1/4K_f \ 0 \ 1/2K_f \ 1/4K_M \\ 1/4K_f \ 1/2K_f \ 0 \ -1/4K_M \\ 1/4K_f \ 0 \ -1/2K_f \ 1/4K_M \\ 1/4K_f \ 1/2K_f \ 0 \ -1/4K_M \end{bmatrix} \begin{bmatrix} U_1 \\ U_2 \\ U_3 \\ U_4 \end{bmatrix} \tag{II.51}$$

Taking the square root of that, the rotors' velocities can be calculated from the control inputs as follows,

$$\Omega_1 = \sqrt{\frac{1}{4K_f}U_1 - \frac{1}{2K_f}U_3 + \frac{1}{4K_M}U_4}$$

$$\Omega_2 = \sqrt{\frac{1}{4K_f}U_1 + \frac{1}{2K_f}U_2 - \frac{1}{4K_M}U_4}$$

$$\Omega_3 = \sqrt{\frac{1}{4K_f}U_1 - \frac{1}{2K_f}U_3 + \frac{1}{4K_M}U_4} \qquad \text{(II.52)}$$

$$\Omega_4 = \sqrt{\frac{1}{4K_f}U_1 + \frac{1}{2K_f}U_2 - \frac{1}{4K_M}U_4}$$

II.6.3 ROTATIONAL EQUATION OF MOTION

Substituting equations (II.46) through (II.49) in equation (II.13), the equation of thetotal moments acting on the quadrotor becomes

$$M_B = \begin{bmatrix} lU_2 \\ lU_3 \\ U_4 \end{bmatrix} \qquad \text{(II.53)}$$

Substituting (II.53) into the rotational equation of motion (II.4) and expandingeach term with their prior definition from this Chapter, the following relation can be derived,

$$\begin{bmatrix} I_{xx} & 0 & 0 \\ 0 & I_{yy} & 0 \\ 0 & 0 & I_{zz} \end{bmatrix} \begin{bmatrix} \ddot{\theta} \\ \ddot{\phi} \\ \ddot{\psi} \end{bmatrix} + \begin{bmatrix} \dot{\theta} \\ \dot{\phi} \\ \dot{\psi} \end{bmatrix} \times \begin{bmatrix} I_{xx} & 0 & 0 \\ 0 & I_{yy} & 0 \\ 0 & 0 & I_{zz} \end{bmatrix} \begin{bmatrix} \dot{\theta} \\ \dot{\phi} \\ \dot{\psi} \end{bmatrix} + \begin{bmatrix} \dot{\theta} \\ \dot{\phi} \\ \dot{\psi} \end{bmatrix} \times \begin{bmatrix} 0 \\ 0 \\ J_r\Omega_r \end{bmatrix} = \begin{bmatrix} lU_2 \\ lU_3 \\ U_4 \end{bmatrix}$$

Expandingthat, leads to,

$$\begin{bmatrix} I_{xx}\ddot{\theta} \\ I_{yy}\ddot{\phi} \\ I_{zz}\ddot{\psi} \end{bmatrix} + \begin{bmatrix} \dot{\theta}I_{zz}\dot{\psi} - \dot{\psi}I_{yy}\dot{\theta} \\ \dot{\psi}I_{xx}\dot{\phi} - \dot{\phi}I_{zz}\dot{\psi} \\ \dot{\phi}I_{yy}\dot{\theta} - \dot{\theta}I_{xx}\dot{\phi} \end{bmatrix} + \begin{bmatrix} \dot{\theta}J_r\Omega_r \\ -\dot{\phi}J_r\Omega_r \\ 0 \end{bmatrix} = \begin{bmatrix} lU_2 \\ lU_3 \\ U_4 \end{bmatrix} \qquad \text{(II.54)}$$

Rewriting the last equation to have the angular accelerations in terms of the other variables,

$$\ddot{\theta} = \frac{l}{I_{xx}} U_2 - \frac{J_r}{I_{xx}} \dot{\theta}\Omega_r + \frac{I_{yy}}{I_{xx}} \dot{\psi}\dot{\theta} - \frac{I_{zz}}{I_{xx}} \dot{\theta}\dot{\psi} \tag{II.55}$$

$$\ddot{\phi} = \frac{l}{I_{yy}} U_3 - \frac{J_r}{I_{yy}} \dot{\phi}\Omega_r + \frac{I_{zz}}{I_{yy}} \dot{\phi}\dot{\psi} - \frac{I_{xx}}{I_{yy}} \dot{\psi}\dot{\phi} \tag{II.56}$$

$$\ddot{\psi} = \frac{1}{I_{yy}} U_4 + \frac{I_{xx}}{I_{zz}} \dot{\theta}\dot{\phi} - \frac{I_{yy}}{I_{zz}} \dot{\phi}\dot{\psi} - \dot{\phi}\dot{\theta} \tag{II.57}$$

To simplify, define,

$$a_1 = \frac{I_{yy} - I_{zz}}{I_{xx}} \qquad a_5 = \frac{I_{xx} - I_{yy}}{I_{zz}}$$

$$a_2 = \frac{J_r}{I_{xx}} \qquad b_1 = \frac{l}{I_{xx}}$$

$$a_3 = \frac{I_{zz} - I_{xx}}{I_{yy}} \qquad b_2 = \frac{l}{I_{yy}}$$

$$a_4 = \frac{J_r}{I_{yy}} \qquad b_3 = \frac{l}{I_{zz}}$$

Using the above definition of a_1 to a_3 and$b_1$to b_3, equations (II.55) through (II.57) can then be rewritten in a simpler form in terms of the system states,

$$\ddot{\Phi} = b_1 U_2 - a_2 x_4 \Omega_r + a_1 x_4 x_6 \tag{II.58}$$

$$\ddot{\theta} = b_2 U_3 + a_4 x_2 \Omega_r + a_3 x_2 x_6 \tag{II.59}$$

$$\ddot{\psi} = b_3 U_4 - a_5 x_2 x_4 \tag{II.60}$$

With the choice of the control input vector U, it is clear that the rotational subsystem is fully-actuated, it is only dependent on the rotational state variables $x_1 to x_6$ that correspond to $\phi,\dot{\Phi},\dot{\theta},\dot{\psi}$ respectively.

II.6.4 TRANSLATIONAL EQUATION OF MOTION

Substituting equations (II.46) through (II.49) in equation (II.15), the equation of the total moments acting on the quadrotor becomes,

$$F_B = \begin{bmatrix} 0 \\ 0 \\ 0 \\ -U_1 \end{bmatrix} \tag{II.61}$$

Embedding that into the translational equation of motion (II.14) and expanding the terms, we get

$$m\begin{bmatrix} \ddot{x} \\ \ddot{y} \\ \ddot{z} \end{bmatrix} = \begin{bmatrix} 0 \\ 0 \\ mg \end{bmatrix} + \begin{bmatrix} c\psi c\theta & c\psi s\Phi s\theta & s\Phi s\psi + c\Phi c\psi s\theta \\ c\theta s\psi & c\theta c\psi + s\Phi s\theta\psi & c\Phi s\theta s\psi - c\psi s\theta \\ -s\theta & -c\theta s\Phi & c\Phi c\theta \end{bmatrix} \begin{bmatrix} 0 \\ 0 \\ -U_1 \end{bmatrix}$$

$$m\begin{bmatrix} \ddot{x} \\ \ddot{y} \\ \ddot{z} \end{bmatrix} = \begin{bmatrix} 0 \\ 0 \\ mg \end{bmatrix} + \begin{bmatrix} -U_1(s\Phi s\psi + c\Phi c\psi s\theta) \\ -U_1(c\Phi s\theta s\psi - c\psi s\theta) \\ -U_1 c\Phi c\theta \end{bmatrix} \tag{II.62}$$

Rewriting Equation (II.62) to have the accelerations in terms of the other variables, we get

$$\ddot{x} = \frac{-U_1}{m}(sinx_1 sinx_5 - cosx_1 cosx_5 sinx_3) \tag{II.63}$$

$$\ddot{y} = \frac{-U_1}{m}(-cosx_5 sinx_1 + cosx_1 sinx_5 sinx_3) \tag{II.64}$$

$$\ddot{z} = g - \frac{-U_1}{m}(cosx_1 cosx_3) \tag{II.65}$$

It is clear here that the translational subsystem is underactuated as it dependant on both the translational state variables and the rotational ones.

II.6.5 STATE SPACE REPRESENTATION

Using the equations of the rotational angular acceleration. Equations (II.58) to (II.60), and those of translation, Equations (II.63) to (II.65), the complete mathematical model

$$\dot{x_1} = \dot{\Phi} = x_2 \tag{II.66}$$

$$\dot{x_2} = \ddot{\Phi} = x_4 x_6 a_1 + b_1 U_2 - x_4 \Omega_r a_2 \tag{II.67}$$

$$\dot{x_3} = \dot{\theta} = x_4 \tag{II.68}$$

$$\dot{x_4} = \ddot{\theta} = x_2 x_6 a_3 + b_2 U_3 - x_2 \Omega_r a_4 \tag{II.69}$$

$$\dot{x_5} = \dot{\psi} = x_6 \tag{II.70}$$

$$\dot{x_6} = \ddot{\psi} = x_2 x_4 a_5 + b_3 U_4 \tag{II.71}$$

$$\dot{x_7} = \dot{z} = x_8 \tag{II.72}$$

$$\dot{x}_8 = \ddot{z} = g - \frac{-U_1}{m}(cosx_1 cosx_3) \tag{II.73}$$

$$\dot{x_9} = \dot{x} = x_{10} \tag{II.74}$$

$$\dot{x_{10}} = \ddot{x} = \frac{-U_1}{m}(sinx_1 sinx_5 - cosx_1 cosx_5 sinx_3) \tag{II.75}$$

$$\dot{x_{11}} = \dot{y} = x_{12} \tag{II.76}$$

$$\dot{x_{12}} = \ddot{y} = \frac{-U_1}{m}(-cosx_5 sinx_1 + cosx_1 sinx_5 sinx_3) \tag{II.77}$$

$$f(X,U) = \begin{bmatrix} x_2 \\ x_4 x_6 a_1 + b_1 U_2 - x_4 \Omega_r a_2 \\ x_4 \\ x_2 x_6 a_3 - b_2 U_3 + x_2 \Omega_r a_4 \\ x_6 \\ x_2 x_4 a_5 + b_3 U_4 \\ x_8 \\ g - \frac{-U_1}{m}(cosx_1 cosx_3) \\ x_{10} \\ \frac{-U_1}{m}(sinx_1 sinx_5 - cosx_1 cosx_5 sinx_3) \\ x_{12} \\ \frac{-U_1}{m}(-cosx_5 sinx_1 + cosx_1 sinx_5 sinx_3) \end{bmatrix} \tag{II.78}$$

II.7 QUADROTOR FLIGHT CONTROL DESIGN

This section presents the process of designing the flight control algorithm for the quadrotor based on the mathematical model developed in the previous Chapter. The PID controller was chosen as the control technique to stabilize (control attitude) the quadrotor model in flight and the method to tune the PID controller is elaborated as well in this section.

II.7.1 CONTROL MODELLING OF QUADROTOR

The control modeling of the quadrotor is summarized and presented in the block diagram as shown in Figure II-7 below.

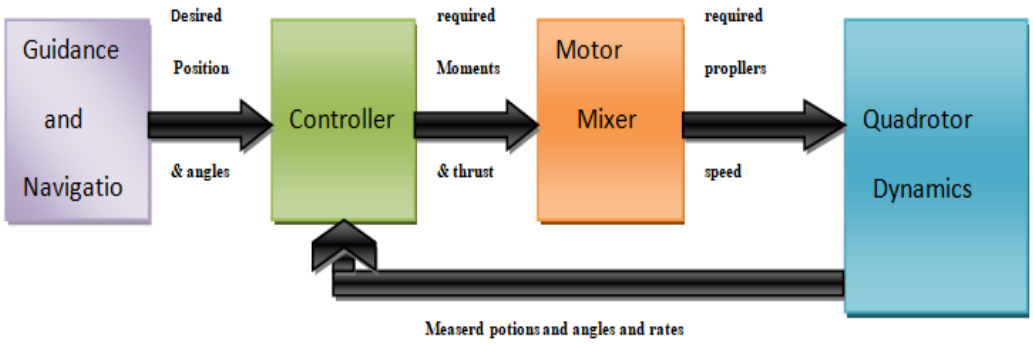

Figure II-7 Block Diagram of Quadrotor Control Model.

- **Trajectory Generator Block**

the trajectory generator block computes the desired flight trajectory that needs to be followed by the quadrotor and generates the set of desired positions (i.e., xd, yd and zd) and desired Euler angles (i.e. ϕd, θd and ψd) in the inertial coordinate frame for that trajectory. If a Remote Control (RC) is used to generate flight command during an actual flight, the trajectory generator block will output the desired Euler angles or their rates to the quadrotor; the choice depends on the control architecture. The desired positions and Euler angles are used as inputs for the controller block to stabilize the Iris+ in flight during the change in the quadrotor attitude (31).

- **Controller Block**

The control of the quadrotor's position and attitude is accomplished by the design of the feedback controller]. As mentioned in the previous section, the quadrotor is an under-actuated system. Therefore, to move forward in the 'x' direction, the quadrotor must first change its attitude by pitching downwards to generate a horizontal force from the propellers' thrusts, while maintaining its altitude. Similarly, in order to move laterally in the 'y' direction, the quadrotor must change its attitude by rolling to the right or left while maintaining its altitude.

- **Motor Mixer**

This block is used to compute the propellers' squared speed from the four basic movement signals. Since the determinant of the movement matrix is different than zero, it can be inverted to find the relation UtoΩ_i^2. The block computation isshown in equation (II.79).

$$\begin{bmatrix}\Omega_1^2\\ \Omega_2^2\\ \Omega_3^2\\ \Omega_4^2\end{bmatrix} = \begin{bmatrix}1/4b & 0 & 1/2bl & 1/4d\\ 1/4b & 1/2bl & 0 & -1/4d\\ 1/4b & 0 & -1/2bl & 1/4d\\ 1/4b & 1/2bl & 0 & -1/4d\end{bmatrix}\begin{bmatrix}U_1\\ U_2\\ U_3\\ U_4\end{bmatrix} \quad \text{(II.79)}$$

- **Quadrotor Dynamics Block**

The required angular speed for each propeller is provided by the motor mixer block to the quadrotor dynamics block as an input and the body response is measured by the sensors onboard the quadrotor as the measured position, Euler angles and their rates. The measured responses are fed back to the controller block and used to determine the error signals for each of the position and Euler angle channel.

II.7.2 SYSTEM CONTROL

The formulated quadrotor model will be used in open-loop simulations and controller design.

II.7.2.1 OPEN LOOP SIMULATION

To verify the mathematical model, an open loop simulation was carried out using MATLAB/Simulink. The quadrotor's parameters were taken from (18). The block diagram for the simulation is shown in Figure II-8.

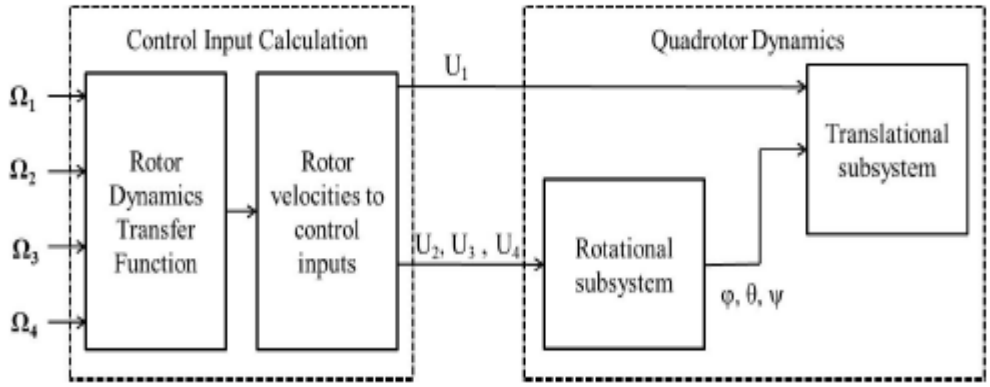

Figure II-8: Open Loop Block Diagram

The rotors speed required for the quadrotor to hover was calculated using the following equation

$$mg = 4F_i$$

$$mg = 4(b\Omega_{ih}^2) \quad \text{(II.80)}$$

Where ih is the hover angular velocity of rotor i.

II.7.2.2 CLOSED LOOP SIMULATION

After the derived mathematical model of the quadrotor was verified using the open loop simulation, the simulation environment is then extended to include an altitude, attitude, heading, and position controllers.

II.7.2.2.1 ALTITUDE CONTROLLER

The open loop simulation previously developed was expanded to include an altitude controller as shown in the block diagram in Figure II-9. The altitude controller takes an error signal $e$as an input which is the difference between the desired altitude $z_d$and the actual altitude z and produces a control signalU_1.

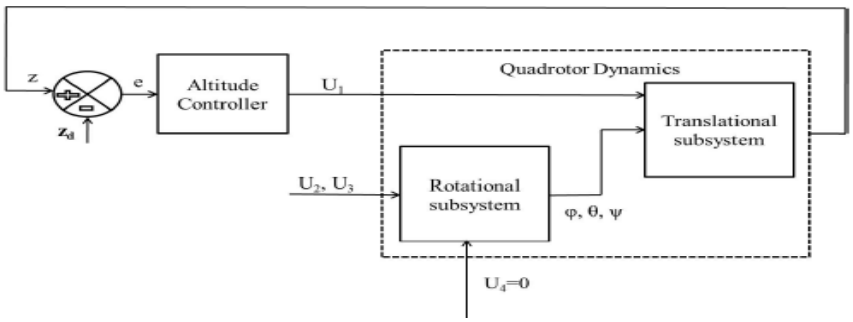

Figure II-9: Block Diagram for Altitude Controller

II.7.2.2.2 ATTITUDE AND HEADING CONTROLLER

To control the attitude and heading of the quadrotor, the open loop simulation wasmodified to include the attitude and heading controllers as shown in Figure II-10.Similar to the attitude controller block, the attitude and heading controller take as an input an error signal$e$which is the difference between the desired rollϕ_d, pitch $\theta_d$and yaw ψ_d and their actual values ϕ, θ and ψ. The attitude and heading controller produces the output signalsU_2, U_3andU_4.

II.7.2.2.3 POSITION CONTROLLER

Unlike the altitude and orientation of the quad rotor, it'sx and y position is notdecoupled and cannot be directly controlled using one of the four control laws U_1throughU_4. On the other hand, the x and$y$ position can be controlled through the roll and pitch angles. The desired roll and pitch angles ϕ_d and $\theta_d$can be calculated from the translational equations of motion, Equations (II.47) and (II.48) as follows:

$$\ddot{x} = \frac{-U_1}{m}\left(\sin\phi_d \sin\psi + \cos\phi_d \sin\theta_d \cos\psi\right)$$

$$\ddot{y} = \frac{-U_1}{m}\left(cos\,\phi_d\, sin\,\theta_d\, sin\,\psi - sin\,\phi_d\, cos\,\psi\right)$$

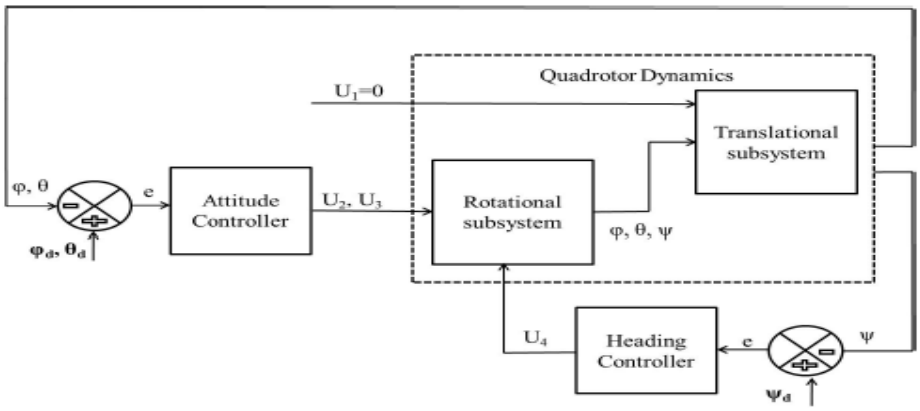

Figure II-10: Block Diagram for Attitude and Heading Controller

Since the quadrotor is operating around hover, which means small values for the rolland pitch angles $\phi$and θ, we can use the small angle assumption ($\sin\phi_d \equiv \phi_d$; $\sin\theta_d \equiv \theta_d$ and $\cos\phi_d = cos\,\theta_d = 1$) to simplify the above equations,

$$\ddot{x} = \frac{-U_1}{m}\left(\phi_d \sin\psi + \theta_d \cos\psi\right) \quad \text{(II.81)}$$

$$\ddot{y} = \frac{-U_1}{m}\left(\theta_d\, sin\,\psi - \phi_d\, cos\,\psi\right) \quad \text{(II.82)}$$

which can be written in a matrix form as,

$$\begin{bmatrix} -\sin\psi & -\cos\psi \\ \cos\psi & -sin\,\psi \end{bmatrix}\begin{bmatrix}\phi_d \\ \theta_d\end{bmatrix} = \frac{m}{U_1}\begin{bmatrix}\ddot{x}_d \\ \ddot{y}_d\end{bmatrix} \quad \text{(II.83)}$$

This can be inverted to get

$$\begin{bmatrix}\phi_d\\ \theta_d\end{bmatrix} = \begin{bmatrix}-sin\psi & -cos\psi\\ cos\psi & -sin\psi\end{bmatrix}^{-1}\frac{m}{U_1}\begin{bmatrix}\ddot{x}_d\\ \ddot{y}_d\end{bmatrix}$$

$$= \frac{m}{U_1}\begin{bmatrix}-sin\psi & cos\psi\\ -cos\psi & -sin\psi\end{bmatrix}\begin{bmatrix}\ddot{x}_d\\ \ddot{y}_d\end{bmatrix} \qquad \text{(II.84)}$$

$$= \frac{m}{U_1}\begin{bmatrix}-\ddot{x}_d sin\psi & +\ddot{y}_d cos\psi\\ -\ddot{x}_d cos\psi & -\ddot{y}_d sin\psi\end{bmatrix}$$

The calculated ϕ_d and θ_d have to be limited to the range between $-20°$ and $20°$ tofulfill the small angle assumption used in the derivation and this can be done via a saturation function in the simulation.

The closed loop simulation for the altitude and attitude controllers is further enhanced to include the position controller as shown in the block diagram in Figure II-11.

The controller blocks in the previous block diagrams can contain any type ofcontrol algorithm, whether linear or nonlinear. All controllers input(s) are the errorrelated to some of the quadrotor's states and produce an output which is either oneor several control inputs U_1 through U_4 or ϕ_d and θ_d if it is the position controller.

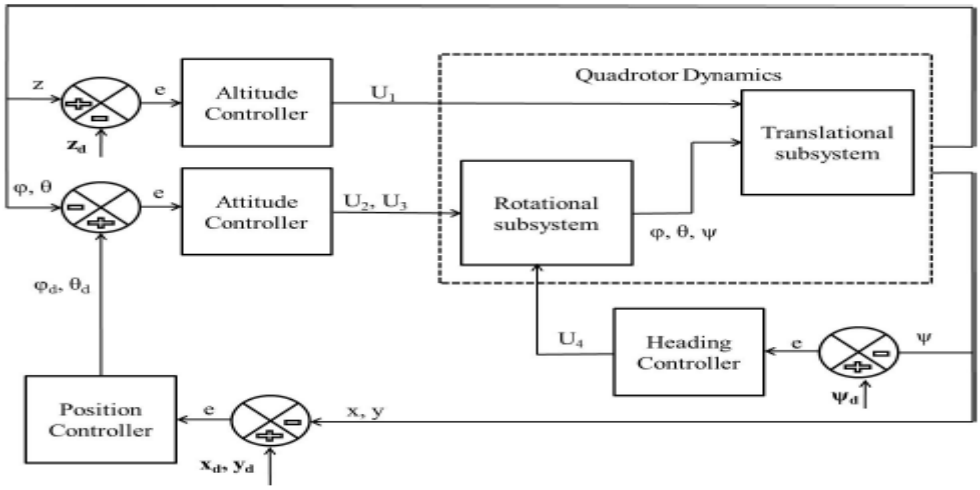

Figure II-11: Position Controller Block Diagram (Complete System)

II.8 Overview of PID Controller

A PID controller consists of three tunable gain values: Proportional gain (i.e. K_P), the Integral gain (i.e. K_I) and the Derivative gain (i.e. K_D) as shown in Figure II-12. The transfer function of a PID controller can be represented by equation (II.85).

$$G_{PID}(s)=K_P + K_I\frac{1}{s} + K_D s \qquad \text{(II.85)}$$

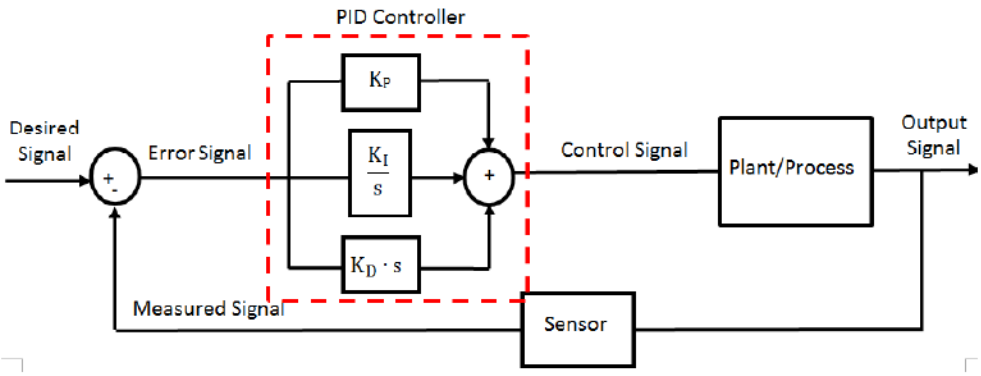

Figure II-12: Illustration of System designed with PID Controller.

Each gain in the PID controller can be tuned to modify a particular transient response parameter of the feedback system (see Figure II-13) and the effects from increasing each gain value separately is further elaborated below:

Proportional Gain, K_P

The K_P value is increased to reduce the time required for the output signal to reach the desired signal (i.e., system response timet_r). By increasingK_P the value alone in the PID controller, a steady-state error can be reduced and expected to be between the desired signal and the output signal. In addition, setting an overly high K_P value will also propagate any inherent disturbance signal within the system and cause the system to undergo unstable oscillations.

Integral Gain, K_I

The K_I value is increased to eliminate the steady-state error of the feedback system. However, as the integral term introduces a pole at the origin of an S-plane plot, the system might

become increasingly unstable when the K_I value is increased (i.e., the system will become increasingly oscillatory in the steady-state).

Derivative Gain, K_D

The $K_D$value is increased to reduce the overshoot, $M_P$and the settling time, t_d of the feedback system's output signal. Although derivative control does not affect the steady-state error directly, it introduces damping to the feedback system. This would allow the system to use a larger K_P value, which would result in improvement to the system's steady-state performance. As described in [8], "derivative control operates on the rate of change of the actuating error and not the actuating error itself this mode is never used alone." Therefore, $K_D$gain is generally used in combination with K_P and K_I control actions.

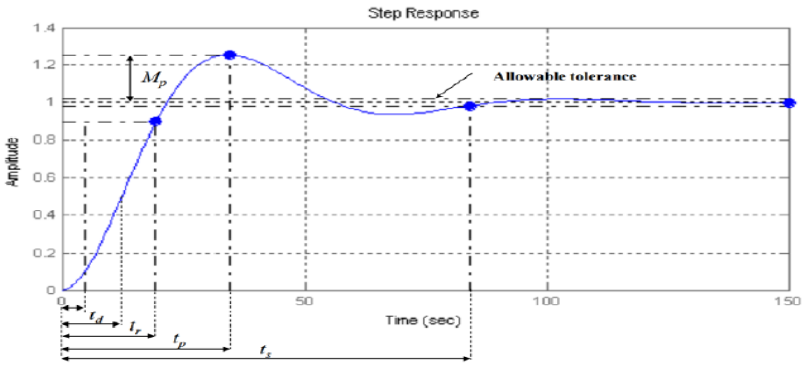

Figure II-13 Transient Response for a Feedback System .

II.8.1 ALTITUDE CONTROL

A PID controller is developed to control the altitude of the quadrotor. It generates the control input U_1 which is responsible for the altitude for the quadrotor as per Equation (II.46). The derived control law is as follows

$$U_1 = k_p(z - z_d) + k_d(\dot{z} - \dot{z_d}) + k_i \int (z - z_d)dt \qquad \text{(II.86)}$$

Where :

k_p : Proportional gain

z_d : Desired altitude

k_d : Derivative gain

$\dot{z_d}$: Desired altitude rate of change

k_iIntegral gain

II.8.2 ROLL CONTROLLER

Another PID controller is developed to control the roll angle Φ of the quadrotor. The derived control law generates the input U_2 that controls the roll angle as follows

$$U_2 = k_p(\Phi - \Phi_d) + k_d(\dot{\Phi} - \dot{\Phi}_d) + k_i \int (\Phi - \Phi_d)dt \quad \text{(II.87)}$$

Where :

k_p : Proportional gain

Φ_d : Desired roll

k_d : Derivative gain

$\dot{\Phi}_d$: Desired roll rate of change

k_i : Integral gain

II.8.3 PITCH CONTROLLER

A PID controller is developed to control the pitch angle θ of the quadrotor. The derived control law generates the input U_3 that controls the pitch angle as follows,

$$U_3 = k_p(\theta - \theta_d) + k_d(\dot{\theta} - \dot{\theta_d}) + k_i \int (\theta - \theta_d)dt \quad \text{(II.88)}$$

Where :

k_p : Proportional gain

θ_d : Desired pitch

k_d : Derivative gain

$\dot{\theta}_d$: Desired pitch rate of change

k_i : Integral gain

II.8.4 YAW CONTROLLER

Similar to the pitch and roll controllers, a yaw controller was developed to generate the control input U_4 based on the following control law,

$$U_4 = k_p(\Psi - \Psi_d) + k_d(\dot{\Psi} - \dot{\Psi}_d) + k_i \int (\Psi - \Psi_d)dt \quad \text{(II.89)}$$

Where:

k_p : Proportional gain

Ψ_d : Desired yaw

k_d : Derivative gain

$\dot{\Psi}_d$: Desired yaw rate of change

k_i : Integral gain

II.8.5 POSITION CONTROLLER

After acquiring stable controllers for the altitude and the attitude of the quadrotor, a complete position controller is developed. PID controllers are used to calculate the desired accelerations $\ddot{x}_d$and $\ddot{y}_d$

$$\ddot{x}_d = k_p(x - x_d) + k_d(\dot{x} - \dot{x_d}) + k_i \int (x - x_d)dt \quad \text{(II.90)}$$

$$\ddot{y}_d = k_p(y - y_d) + k_d(\dot{y} - \dot{y_d}) + k_i \int (y - y_d)dt \quad \text{(II.91)}$$

Where:

k_p: Proportional gain

x_d : Desired x position

k_d : Derivative gain

$\dot{x_d}$: Desired x position rate of change

y_d: Desired y position

$\dot{y_d}$: Desired y position rate of change

k_i : Integral gain

Plugging the values of the desired accelerations$\ddot{x}_d$ and $\ddot{y}_d$ into Equation (II.5), thedesired roll and pitch angles $\Phi$and θ can be calculated which are in turn fed to the attitude controller previously expressed in Equations (II.7) and (II.8).

II.9 PID Controller Simulation Results

II.9.1 ALTITUDE RESPONSE

The controller gains to track the desired generated altitude were as follows:$k_p = 5; k_d = 10$and$k_i = 0$, the integral gain was settling to zero because no steady state error was observed, by that the PID controller was simplified to a PD controller.

The system response is shown in figure II-14(a) while figure II-14(b) shows the altitude response's error and the analysis of this response is shown in the table below 2.1:

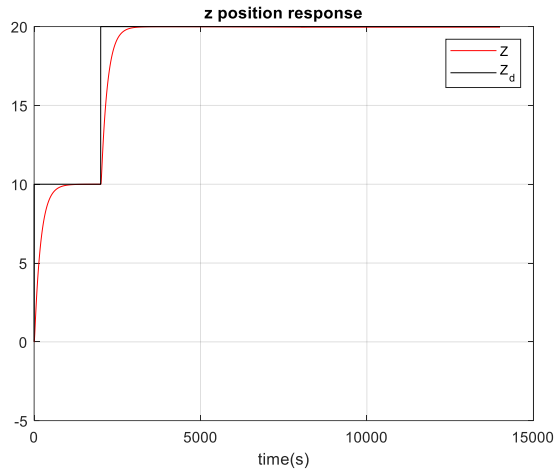

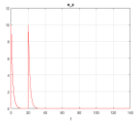

(a) Altitude response (b) the error in altitude

Figure II-14:altitude response

Over shoot	Under shoot	Time response
0.05%	0%	5.5 s

Table II.1: altitude control results

II.9.2 ATTITUDE RESPONSE

The goal from the controller design is to track the desired x, y and z position with stabilize attitude (roll and pith angles) and specific heading(yaw angle) for that the controller gains were as

follows: :$k_p = 10$; $k_d = 20$ and $k_i = 0$, according to these gains the controller is simplified to a PD controller as well. The system response is shown in figure II-15, and the results are well presented in table 2.2.

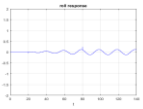

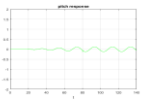

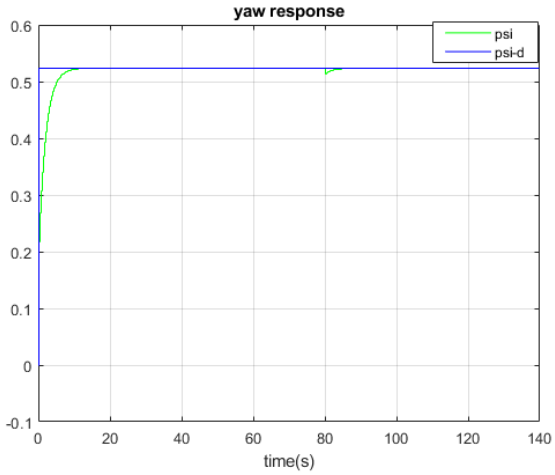

(a) Attitude response (b) headingresponse

Figure II-15: attitude and heading response

	Max & Min	overshoot	Time response
Attitude	-0.12<<0.24	--	--
Heading	--	0.05%	3.5 s

Table II.2: attitude and heading control results

II.9.3 POSITION RESPONSE

The controller gains to track the desired generated X and Y position were as follows: $k_p = 5$; $k_d = 10$ and $k_i = 0$, the system response is shown in figure II-16(a) while

figure II-16(b) shows the altitude response's error and the analysis of this response is shown in the table below II.3:

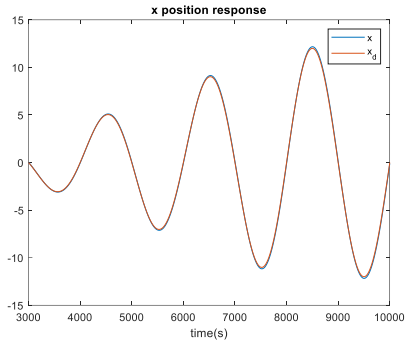

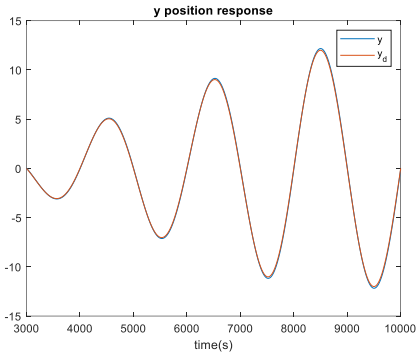

X positin response

Y positin response

Figure II-16: altitude response

	Max	**Min**
X position error	0.20	-0.20
Y position error	0.204	-0.209

Table II.3: position control results

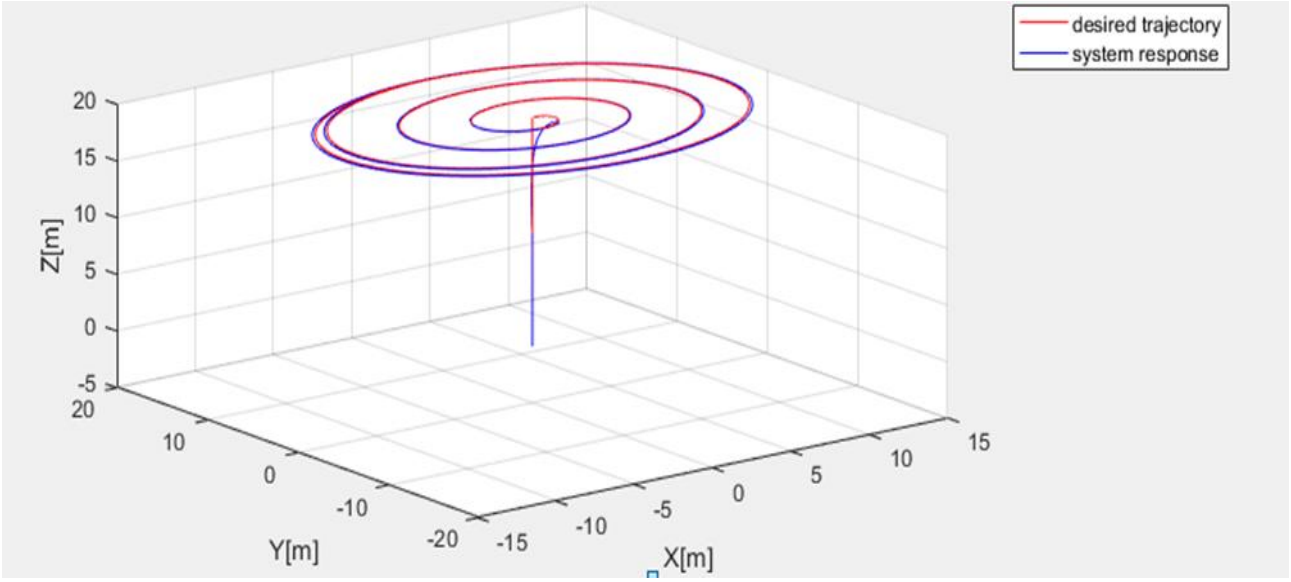

Figure II-17: trajectory response under PD controller

II.10 CONCLUSION

First from these results, we can obviously see that the controller for the pitch rotation is equivalent to that of the roll rotation due to the symmetry of the quadrotor, this theory was verified and proved using the closed loop simulation. As with the roll and pitch, the performance of the y position controller was the same as the performance of the x position controller due to the symmetry of the quadrotor.

In general, term the system response in altitude; position; heading and attitude was stable so the PD controller showed a good performance to stabilize our quadrotor.

III. CHAPTER : PATH PLANNING AND OBSTACLES AVOIDANCE

III.1 INTRODUCTION

Autonomous degree is an important index of UAV's performance. Indoor UAV with high-precision autonomous navigation function release controllers from complicated control work to focus on target search and identification. Path planning is one of the most important problems of autonomous navigation. Path planning problem is to select an optimal collision-free path from a given start location to a destination in obstacle environment based on a certain evaluation criterion.

According to the degree of intelligence in the process of path planning, mobile robot path planning can be divided into traditional path planning and intelligent path planning. The traditional path planning algorithm includes simulated annealing algorithm (19), potential function theory(20), fuzzy logic algorithm (21)and so on. However, these traditional methods can't be further improved in path search efficiency and path optimization. Intelligent path planning algorithm includes Ant Colony Optimization (ACO)(22), genetic algorithm(21), neural network and particle swarm algorithmand so on. The ant colony algorithm has the advantages of strong robustness, good global optimization ability and inherent parallelism. Moreover, it easily combines with multiple heuristic algorithms to improve the performance of algorithms. So it is widely used in path planning.

In this chapter we will generate an optimized path for our quadrotor and free from obstacles based on ACO algorithm.

III.2 THE ACO ALGORITHM

The ant colony algorithm was introduced in the early 1990 s as a new technique for solving combinatorial optimization problems. It is a kind of simulation based on ant behavior and communication and a type of swarm intelligence heuristic algorithm that is based on the study of ant foraging behavior, forming a bionic algorithm currently in the early stages of its life cycle. Initially proposed by Marco Dorigo in 1992, it draws its inspiration from the paths carved by ants searching for food. The positive feedback mechanism is adopted to converge the search process and finally approximate to an optimal solution. The basic principle of applying the ant colony algorithm to the path planning problem is that the optimal solution is represented by a walking path of the ant while all the paths of the whole ant colony constitute the solution space. Under similar conditions, the concentration of the pheromone released by the ants on the shorter path is relatively high. With time, the accumulated pheromone concentration on the shorter path gradually increases, and the

number of ants choosing this path, in turn, also increases. Finally, the whole ant colony focuses on the optimal path under the action of positive feedback (23)(see figure III-1).

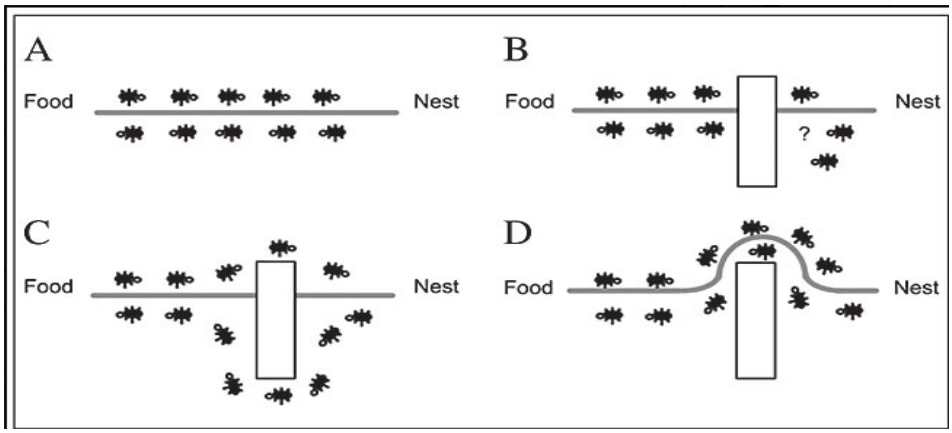

A.ants in a pheromone trail between nest and food; **B**.an obstacle interrupts the trail; **C**. ants find two paths to go around the obstacle; **D**. a new pheromone trail is formed along the shorter path.

Figure III-1: inspiration from ants path planning and obstacle avoidance.(24)

III.2.1 ENVIRONMENT MODELING

The work environment is built by using the grid model, which divides the robot working space into $N^{*}N$ squares. As shown in figure III-2, the gray grids are represented as obstacles (the grid with barriers) and the white grids are represented as free grid squares (the robot can move). In order to identify obstacles, the white grid cell is represented by 0 and the gray grid unit is represented by 1. The grid method is simple and effective to create and maintain grid model. Moreover, the grid method has strong adaptability for obstacle. This method is convenient for computer storage and processing.

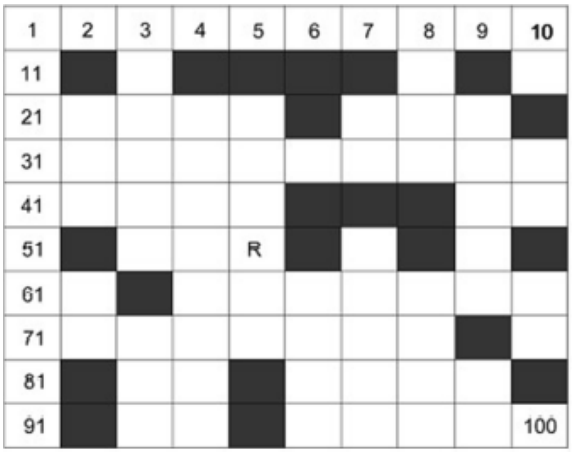

Figure III-2:environment model(25)

The grid model was placed into two-dimensional coordinate system. And then serial number method is adopted to mark each grid. In N^*N grid map, the starting node is named after Start and the target node is named after Goal. The position coordinates (x, y)corresponding to any grid whose grid number is R as follow:

$$\begin{cases} x = \begin{cases} mod(R,N) - 0.5 & if\ mod(R,N)! = 0 \\ N + mod(R,N) - 0.5 & otherwise \end{cases} \\ y = N + 0.5 - ceil\left(\frac{R}{N}\right) \end{cases} \quad \text{(III.1)}$$

Where mod is the surplus operation, $ceil$ rounds the elements to the nearest integers toward infinity.

The distance of two cells is calculated by the length of the line connecting the centers of them, denoted as $d(i, j)$, which is computed by formula (III.2).

$$d_{ij} = \sqrt{(x_i - x_j)^2 + (y_i - y_j)^2} \quad \text{(III.2)}$$

Wherever the UAV is in, the next cell to visit is adjacent to the current cell. It could be on any side: above, below, left, right, front, back, or diagonally adjacent. There are 8 directions to move at most(see figure III-3).

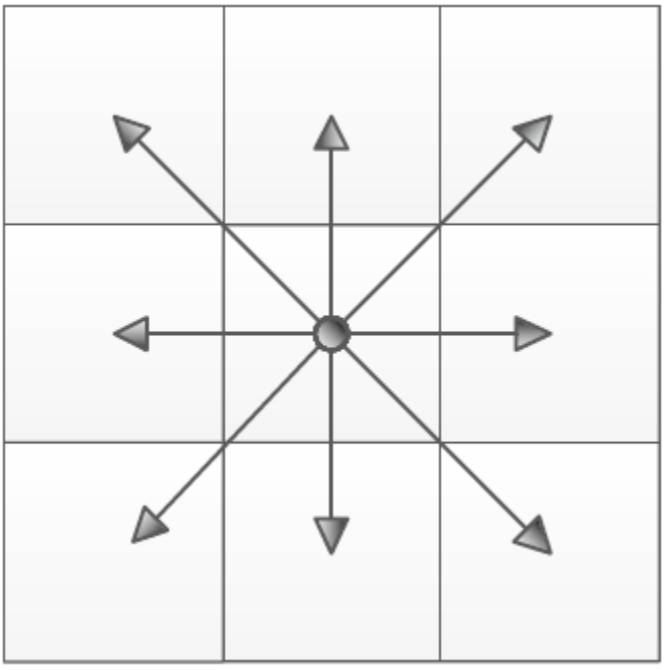

Figure III-3: possible directions for UAV(26)

III.2.2 METHODOLOGY

III.2.2.1 BASIC PRINCIPLE OF ACO ALGORITHM

Ants are social insects that live in colonies in which they cooperate with each other to find food sources. It was found that they, communicate with each other by laying down a kind of aromatic essence called pheromone on the path they have travelled [12]. Assume there are two paths, path A and path B, are available for the ants to travel from their nest to the food sources. Path A is shorter than path B. Initially, as there is no pheromone trail on both paths, ants pick one path randomly. The ants on path A will reach the food resources earlier. When returning the nest, each ant reselects a path. The ants who select path A will always finish their travel in a shorter time. As a consequence, pheromone concentration on path A increases faster than that on path B. Other ants, observing the pheromone trail, are attracted to follow path A. Then pheromone concentrate on path A will be stronger therefore attracts more ants. Finally, as a result of the positive feedback, most ants select path A. Path A is selected to be the best path by the ant colony. ACO algorithm shapes up by imitating the foraging process of ants described above. It has advantages of positive feedback of information, high parallelism, and optimization capability. Additionally, the foraging process of ant colony is quite similar with the path planning of UAV. Both of them are finding a best collision-free path from the start location to the destination. Thus the ACO algorithm is a good candidate to tackle the UAV path planning problem. Meanwhile, the algorithm has shortcomings such as low efficiency in the initial stage for the lack of pheromone, and easily trapped into local optimal solution.

III.2.2.2 PATH PLANNING BASED ON ACO ALGORITHM

To simulate the foraging behavior of actual ant, consider the start location of UAV as the ant nest, and the destination of UAV as the food source. The process of UAV path planning based on ACO algorithm is to find the best path to the food source through the cooperation of ants.

Some notations and assumptions are presented as follows:

1) $Ant = \{1,2\ldots,k,\ldots,m\}$ is the ant group, of which m is the amount of the ants and k is one of the ants.
2) Defined an array structure called tabu list for each ant to record the cells which have been visited. For each ant, revisit a cell in the list is forbidden. Another function of the list is to

calculate the length of path when an ant finishes its travel. The tabu list is notated as*ant(i).visited (i=1,2,...,m).*

3) Array *allowed* is the candidates group for the next step which varies as the location changes. Every time when an ant reach a new cell, search the adjacent cells, those cells, except the occupied ones and cells in tabu list, are the candidates.
4) Pheromone level of any edge is stored in matrix τ .τ (*i, j*) indicates the pheromone level on edge between cell i and cell j and could be notated asτ_{ij}. All elements are initialized at 0τ.

Put m ants on the start cell. Each ant takes the current cell as a center and then selects a cell for the next step from their selectable cells group based on a given criterion. The criterion is called random proportional rule. At time t, the probability for ant k selecting the path from cell i to j is calculated by formula (III.3).

$$P_{ij}^{k}(t) = \begin{cases} \dfrac{\tau_{ij}^{\alpha}(t).\eta_{ij}^{\beta}(t)}{\sum_{s\epsilon\ allow\ k}\tau_{is}^{\alpha}(t).\eta_{is}^{\beta}(t)} & s \in allow_k \\ 0 & s \notin allow_k \end{cases} \qquad \text{(III.3)}$$

With

$$\eta_{ij}(t)=\frac{1}{d_{ij}}$$

Where τ_{ij}Is the pheromone trail of the path grid i to grid j, and ηij is the heuristic information of the path grid i to grid j. αis the stimulating factor of pheromone concentration which determine the relative influence of the pheromone trail. βis the stimulating factor of visibility which determine the relative influence of the heuristic information. $allow_k$is the collection of grids which ants can choose when ants in the grid i (in other words, they are the grids around the grid i except the obstacle grid and tabu grid).

In order to simulate the change of pheromone in the process of ant foraging, the update of artificial ant colony pheromone also considers the two processes of volatilization and release of pheromone. In the real world, as time goes by, the pheromone on the path will gradually evaporate. And its volatilization is helpful for ants to explore other areas to find better paths, so it does not converge too quickly to a local optimal solution; in the path of ants to explore food, the corresponding pheromones are also released, so that the ants can communicate with each other and have a certain guiding effect on other ants who are looking for food. The initial setting of the pheromone is neither too large nor too small; too large will make its guiding effect lower, while too

small will make the ant group converge too quickly to a local optimal path .Thus, the pheromone update formula (III.4) is expressed as follows:

$$\tau_{ij}(t) = (1-\rho)\tau_{ij}(t) + \sum_{k=1}^{m} \Delta\tau_{ij}^{k} \qquad \text{(III.4)}$$

Where $0 < \rho \leq 1$the evaporation is rate of the pheromone and is usually set to 0.5 in the ACO. Therefore,$(1-\rho)\tau_{ij}(t)$ represents the residual amount of a path pheromone found by the ant after volatilization, and $\Delta\tau_{ij}^{k}$ is the pheromone left by the k^{th} ant in the path i to j. As shown in Eq. (III.5):

$$\Delta\tau_{ij}^{k} = \begin{cases} (C_k)^{-1} & ,shortest\ path \\ 0 & ,otherwise \end{cases} \qquad \text{(III.5)}$$

Where $C_k$is the total path length obtained after the k^{th} ant walks the complete path. Here, as described above, the optimal path distance is obtained.

III.2.2.3 FLOWCHART OF ACO

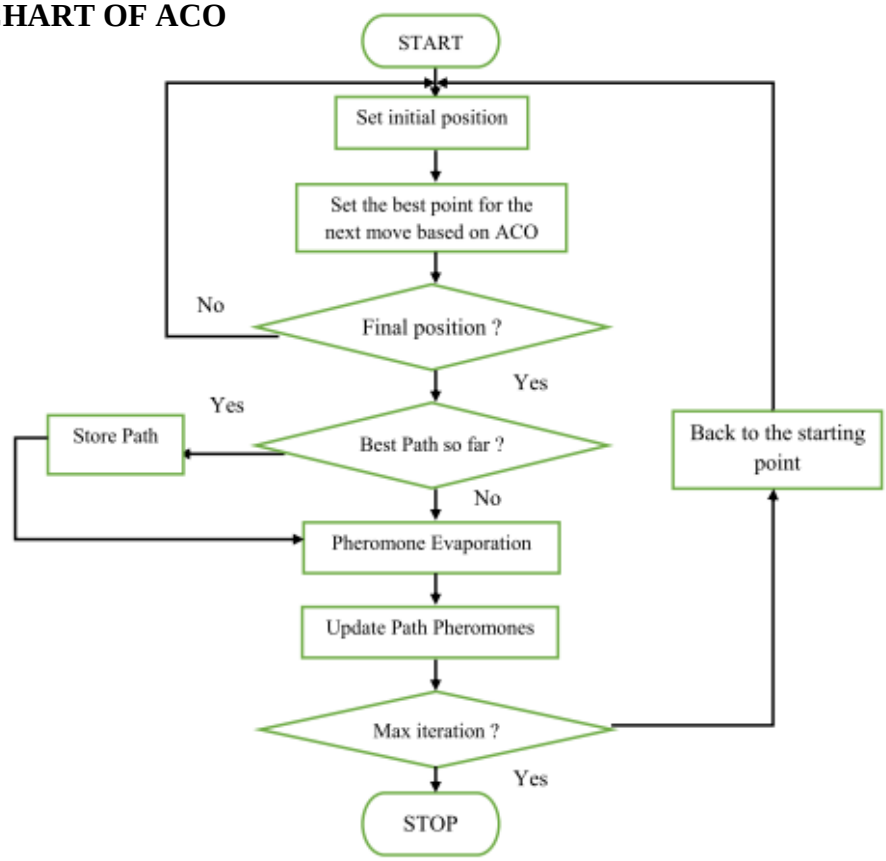

Figure III-4: Computational flowchart of ACO

III.3 SIMULATION RESULTS

In this section the simulation related to the quadrotor's optimal trajectory generation and control are performed in MATLAB/Simulink. The PID controller developed in the previous chapter was used to stabilize the quadrotor while tracking the generated path.

The workspace is modeled in a grid map with 10*10 grids as shown in figure III-2. The path planned based on ACO algorithm shown in figure III-5 is only in x(figure III-6) and y (figureIII-7) coordinates, so after tracking the desired altitude this 2 dimension path is implemented to the trajectory generator block presented in chapter 2 to be tracked as well.

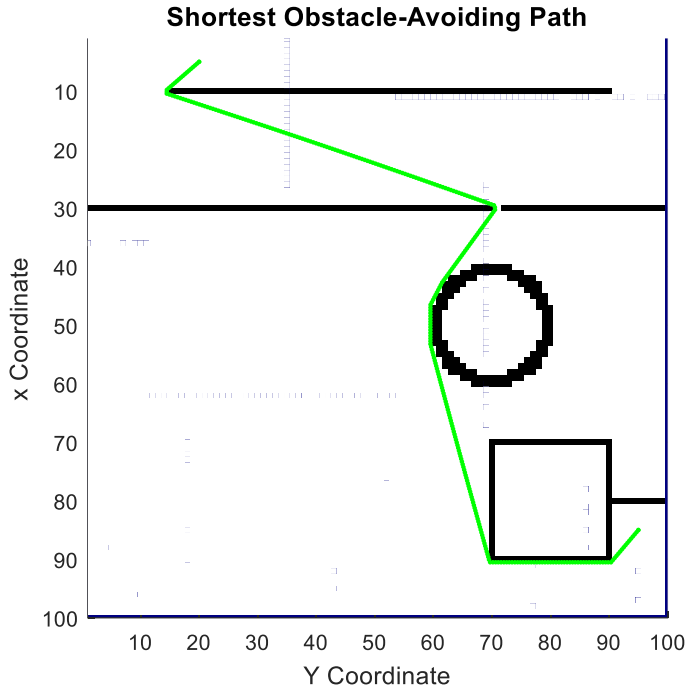

Figure III-5: The shortest path based on ACO algorithm

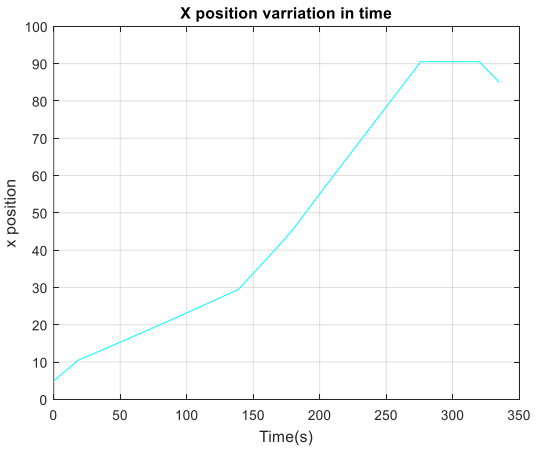

Figure III-6: the generated x position

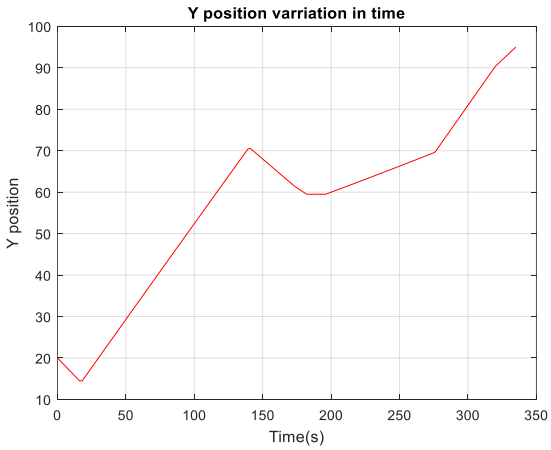

Figure III-7: the generated y position

SYSTEM RESPONSE:

The system response for tracking the optimized path with avoiding obstacles is shown in figure III-7 to figure III-10 in details.

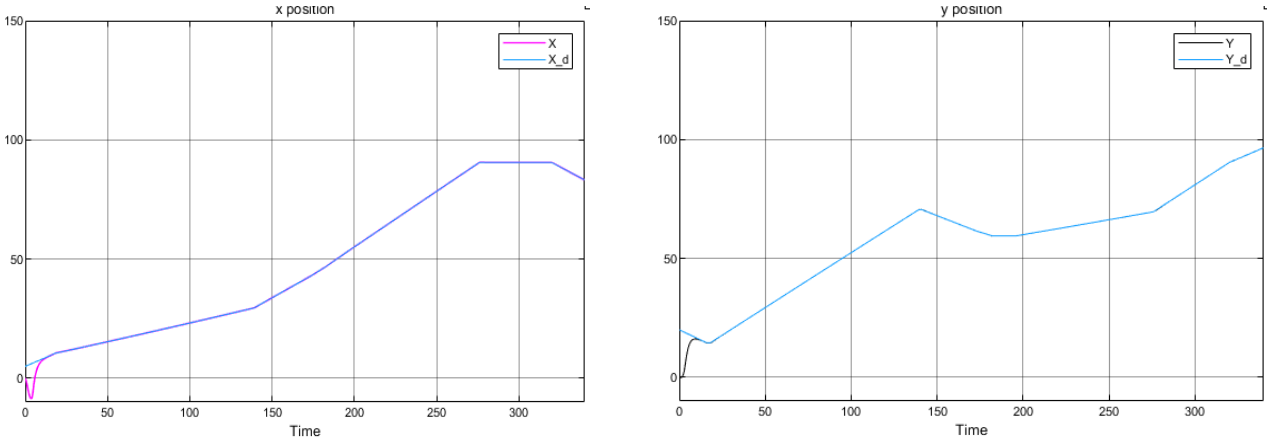

(a) tracking the generated x position (b) tracking the generated y position

Figure III-8: the position response

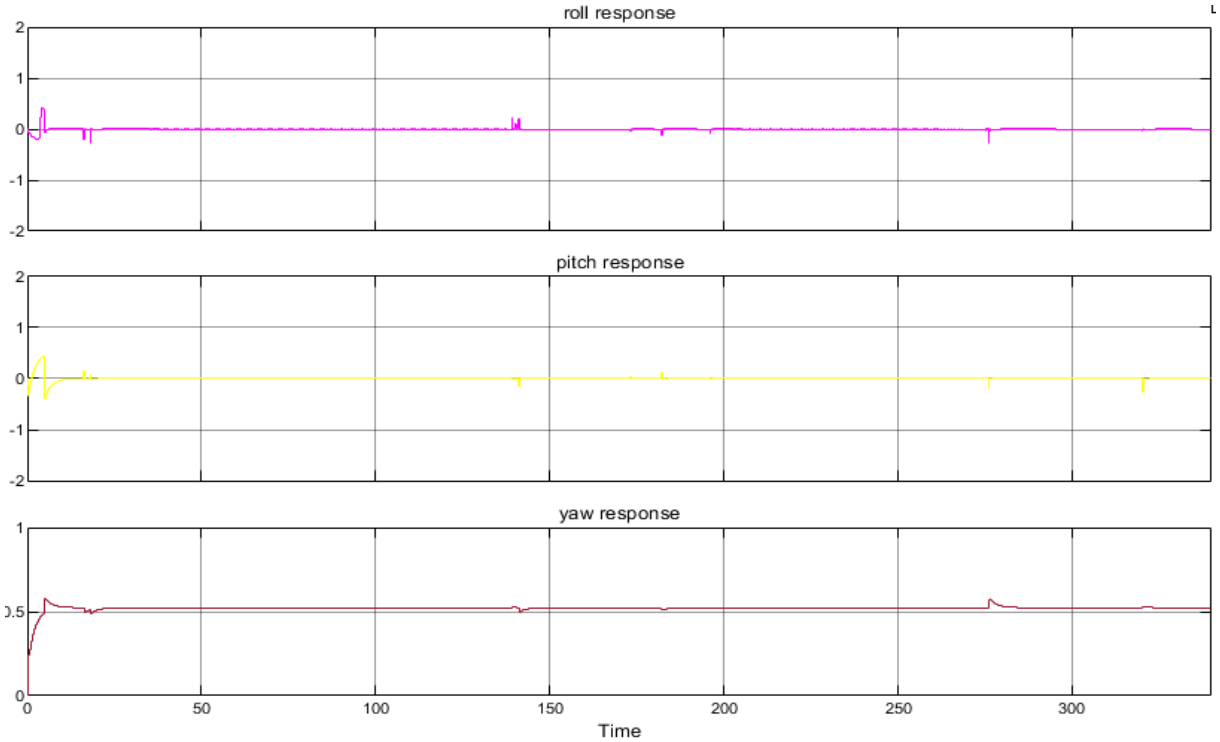

Figure III-9: the attitude and heading response

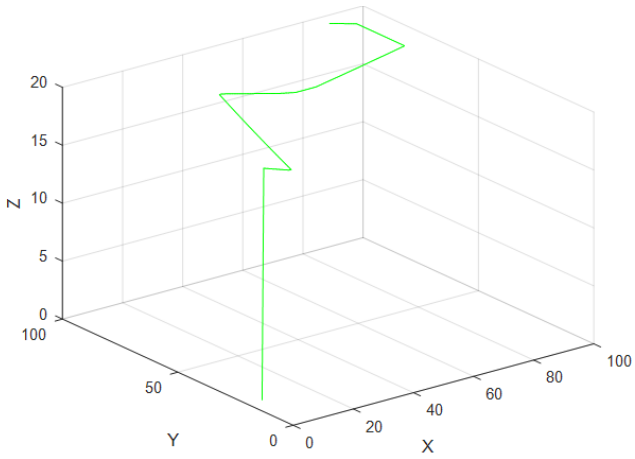

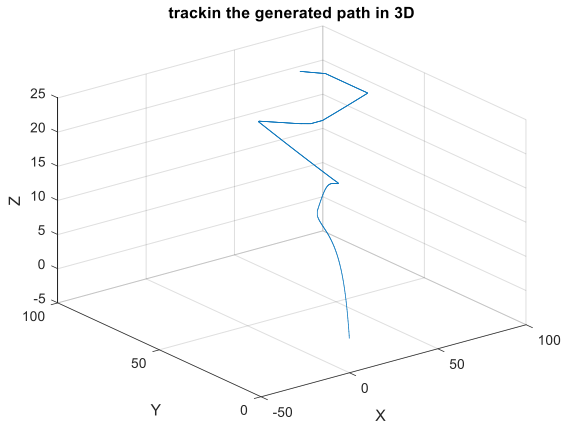

The desired path in 3D System response in 3D

Figure III-10: system response to the generated path in 3D

III.4 CONCLUSION

According to the results the ACO algorithm showed a good performance in creating a short path while avoiding obstacles, the quadrotor response when tracking the generated path was stabilized after an undershooting in x and y position due to the limitation of the PID controller in the first seconds, after that the position errors converge to zero and the attitude was well maintained .

IV. CHAPTER : QUADROTORS FORMATION CONTROL

IV.1 INTRODUCTION

Multiple or cooperative UAVs can be defined as a group of vehicles having the same objectives in common cooperation to ensure mission execution successfully, with better performance than single vehicle. These vehicles can perform this task while maintaining a certain formation shape with constant relative distances. Formation shapes have been carried out using much architecture. Leader-follower, behavioral and virtual structure are the mostly used approaches. In leader follower approach, one or more robots act as a leader while the others are followers. The leader robot tracks a certain trajectory, while the followers are placed at certain distance from the leader to produce the required formation (33).

In this chapter we will present the different strategies of formation control and give a final conclusion of this work presented in this thesis.

IV.2 FORMATION CONTROL

The predefined trajectory for the group of UAVs is called "formation trajectory". It represents the common interest of the group of quadrotors. Considering the formation trajectory, we give the definition about the formation task as follows:

Definition: $Formation\ task$: $A\ formation\ task\ for\ a\ multi-quadrotor\ system\ with\ L-F\ architecture\ is\ represented\ by\ a\ desired\ formation\ trajectory\ (given\ to\ the\ leader(s))\ and\ a\ desired\ geometric\ pattern\ (desired\ interdistance\ and\ orientation\ between\ neigh-boringquadrotors)\ for\ the\ group\ of\ quadrotors.$

In the above definition, the formation task is rigid if the desired geometric pattern is fixed. Otherwise, the formation task is flexible. The formation task describes the desired integral behaviors of the multiple quadrotors. The objective of the formation control is to accomplish the formation task, i.e., the quadrotors keep the desired pattern and track a given trajectory by using the formation controllers. The formation control strategies are based on the formation structures. According to the different formation structures, which we detail the following three formation control strategies, i.e., the hierarchical centralized, decentralized and distributed formation control strategies (14).

IV.2.1 HIERARCHICAL CENTRALIZED FORMATION CONTROL

IV.2.1.1 CENTRALIZED CONTROL WITHOUT LEADER IN THE FORMATION

This formation control strategy is considered as a quantitative extension with respect to the single quadrotor navigation problem. The formation is achieved through the planning of the desired trajectory of each quadrotor. The planed trajectories of the quadrotors should be tracked perfectly thus the collisions are avoided during the formation. In this case, a central decision maker exists to generate the desired trajectories for the agents. This formation control strategy is considered as, which is commonly based on a central trajectories generator.

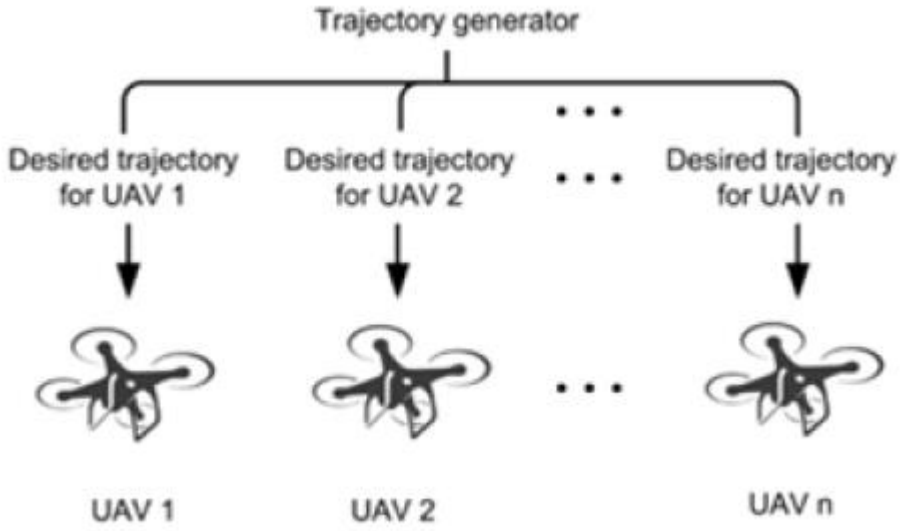

Figure IV-1: Centralized control without leader in the formation(14)

This method is a completely centralized method, which is then simple and quite easy to implement because no interaction between UAVs is considered. However, a wide bandwidth communication channel and fast processors are required to guarantee the performance of the system. The centralized method is known as an efficient and simple implementation approach. This formation control structure can be depicted in Figure IV.1

IV.2.1.2 HIERARCHICAL CENTRALIZED FORMATION CONTROL WITH L-F CONFIGURATION

As shown in Figure IV.2, the desired formation trajectory is given to some of the quadrotors in the group, designed as leaders of the group. The position and orientation states of the leaders are transferred to the followers through communication modules.

This strategy reduces the burden of the central component. The calculation and data transmission are shared by some low-level components. The collision avoidance does not need to be considered explicitly, if the controllers are well-designed.

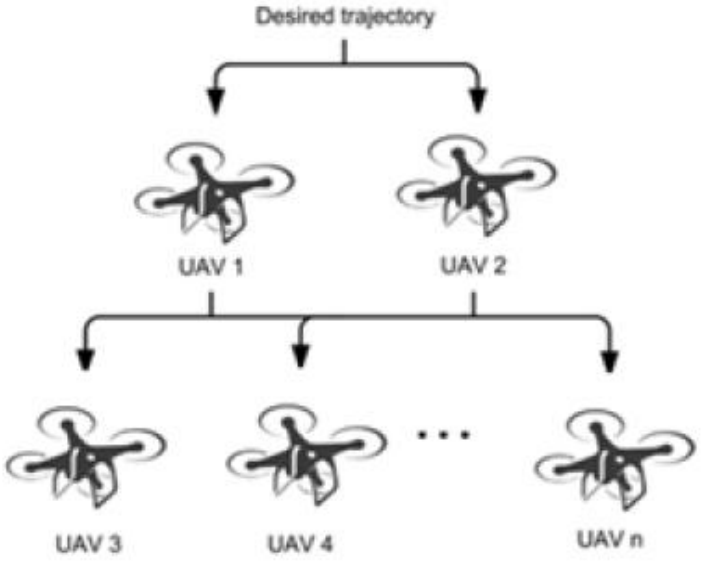

Figure IV.2: Centralized formation control with L-F configuration(14)

IV.2.2 DECENTRALIZED FORMATION CONTROL

As shown in Figure IV-3, for this formation structure, the leader does not exist. The desired position or trajectory is predefined for each quadrotors. The navigation of the quadrotors is achieved based on the ‘’navigational feedback”. Every quadrotors should have the ability of sensing/detecting other UAVs around them for the collision avoidance .

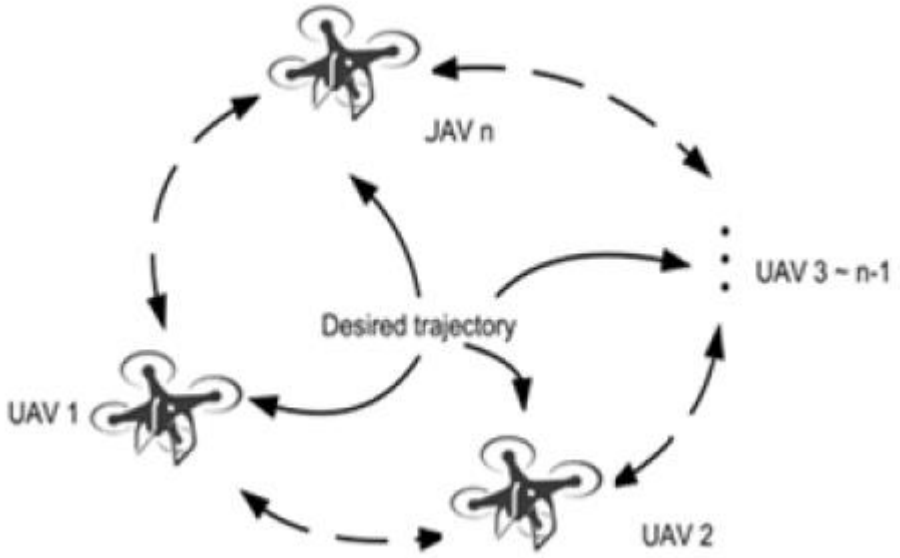

Figure IV-3:Decentralized formation control(14)

The dashed lines in Figure IV-3 represent the possible detections between the UAVs. The idea is to keep some inter-distances between the UAVs, specially when the system is in the presence of disturbance.

IV.2.3 DISTRIBUTED FORMATION CONTROL

The distributed formation control structure evolves from the decentralized structure The terminology “distributed” is usually used in the domain of computer science. In multi-robot systems, the term “distributed” is used, when the communication issues are added between the robots. Distributed control is related to the areas of decentralized control and of large scale systems. Distributed control strategies have been proposed to include communication issues into the decentralized control design framework. Such extensions concern the communication among subsystems, local controllers, and communication in the feedback loop (34).

IV.2.4 DECENTRALIZED/DISTRIBUTED FORMATION CONTROL WITH L-F

An example of the L-F decentralized formation structure is depicted in Figure IV-4 the red quadrotors represent the leaders (In some special formation task, the leadersare changeable), while the others are followers. The difficulty of this formation structure is that the followers have no knowledge about the formation trajectory .

They only depend on the states of their neighbors (positions and velocities) in order to accomplish the formation task. Therefore, the interactions are important for the followers, not only

for the reason of collision avoidance but also for the reason of formation. The proposed leader-follower formation has the following novelties comparing to the existing works (32).

- Decentralized formation control: no single centralized decision maker (e.g. external trajectory generator) exists. The quadrotors do not have any global knowledge.
- Multiple and changeable leaders: the number of leaders may be greater than one; the statue (leader or follower) of the agent is changeable.
- Interactions between leaders and followers: the leader(s) can be affected by their neighboring followers.

Note1.

In the investigated leader follower formation problem, only the leader is aware of the formation taskthe remaining UAVs interact with each otheror with the leaders through a rigidor switching topology.

Note2.

The rigid or switching topology does not correspond to the rigid or flexible formation. Although a formation is rigid, it may have rigid or switching topology.

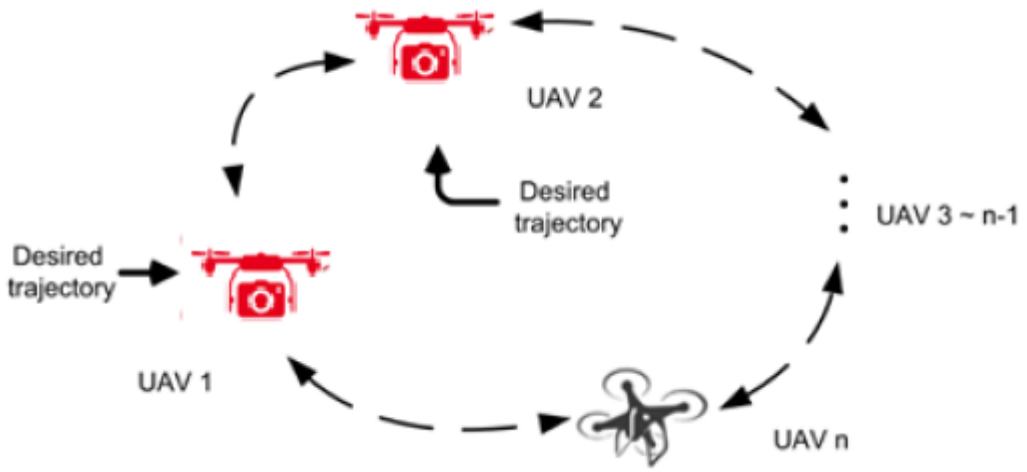

Figure IV-4: Distributed formation control with L-F configuration(14)

IV.3 CONTROLLER DESIGN

In this section a control formation scheme is proposed in order to maintain the centralized Leader-followers formation. Considering a team of i quadrotors under a leader-follower approach, such that $i\epsilon$ (L; 1; 2; 3; ….. N), where L is the leader while N are the number of followers (27).

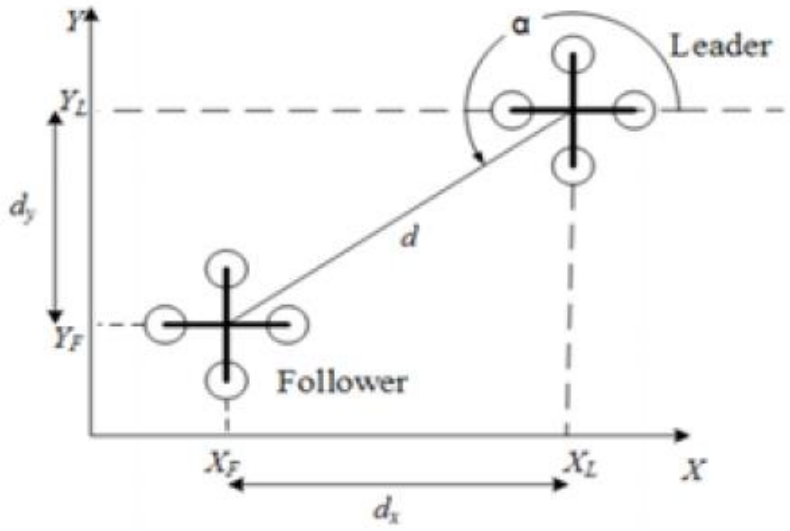

Figure IV-5: Leader-followers formation architecture(27)

The objective of the formation controller is to achieve the desired leader-follower formation configuration in X-Y plane, after following the leader in the Z direction to either same or different height. This formation shape is maintained via keeping a constant distance d and angle between each follower and the leader.

$$d_x = -(X_L - X_F)cos\psi_L - (Y_L - Y_F)sin\psi_L$$
$$d_y = -(X_L - X_F)sin\psi_L - (Y_L - Y_F)cos\psi_L \quad \text{(IV.1)}$$

with $d_x$and d_x and $d_y$are the X and Y coordinates of the actual distance d as shown in Figure IV-5 The proposed control algorithm is shown in Figure IV.6 applying SMC in its design to keep the formation even in perturbed and uncertain environment. Formation control errors of x; y and z should satisfy the following conditions:

$$\lim_{t\to\infty} \|e_x\| = \left\|d_x^d - d_x\right\| = 0$$
$$\lim_{t\to\infty} \left\|e_y\right\| = \left\|d_y^d - d_y\right\| = 0 \quad \text{(IV.2)}$$

Where $d_x^d \; and \; d_y^d$ are the desired distance between the leader and follower in the X and Y coordinates respectively (35).

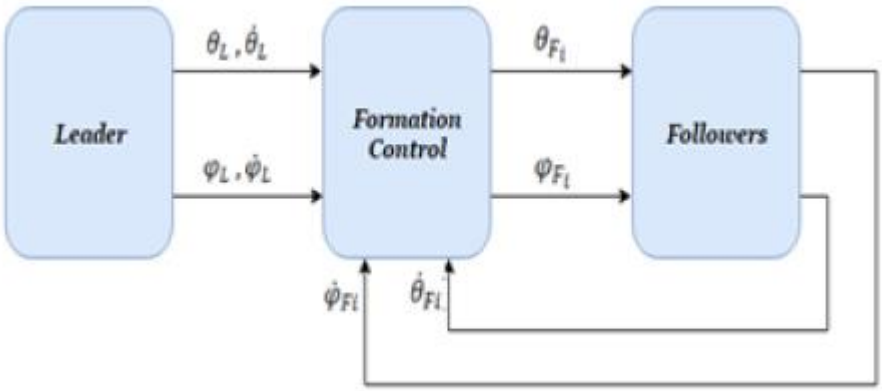

Figure IV-6: Leader-followers formation controller(27)

To achieve this goal, first-order sliding mode controller is used to minimize this error. First, a time varying surface S (t) is defined by the scalar equation s(e; t) = 0, where:

$$S(e,t)=(\frac{d}{dy}+\lambda)^{n-1}e \tag{IV.5}$$

The second-order tracking problem can be transferred to a first-order stabilization problem, thus:

$$\begin{aligned} \dot{s} &= \ddot{e} + \lambda \dot{e} \\ \frac{1}{2}\frac{d}{dy}s^2 &\leq -\eta|s| \end{aligned} \tag{IV.6}$$

Equation IV.6 is a Lyapunov candidate function chosen for the control law u to maintain scalar s = 0. This function states that s^2 is the squared distance to the sliding surface, where ηa positive constant is. The formation can be then controlled for each follower using the following equations:

$$\begin{aligned} \ddot{X}_{Fi} &= \ddot{X}_L + \lambda_x(\dot{X}_L - \dot{X}_{Fi}) \\ \ddot{Y}_{Fi} &= \ddot{Y}_L + \lambda_x(\dot{Y}_L - \dot{Y}_{Fi}) \end{aligned} \tag{IV.7}$$

Finally, the position control problem is transformed to an attitude control, which means that a direct estimation of the attitude can be used to control the swarm:

$$\theta_{Fi} = \theta_L + \lambda_\theta(\dot{\theta}_L - \dot{\theta}_{Fi})$$
$$\phi_{Fi} = \phi_L + \lambda_\phi(\dot{\phi}_L - \dot{\phi}_{Fi}) \quad \text{(IV.8)}$$

Where$\lambda_\theta$and $\lambda_\phi$are the formation control gains, with λ_θ>0 and λ_ϕ>0.

IV.4 THE SIMULATION RESULTS

The simulation results related to the quadrotors formation control is presented in this section. three quadrotors are used in simulation, a leader and two followers. The leader begins its route by following the required height z first from its initial position, then following the required track in $X-Y$ plane. The followers's desired formation distance with respect to the leader are $d_{F1}^d = [5,-5,0]^T$and $d_{F2}^d = [-5,-5,0]^T$.

As shown in Figure IV-7 and IV-8, it is clear that the UAVs team succeeds in following their leader with the required formation.

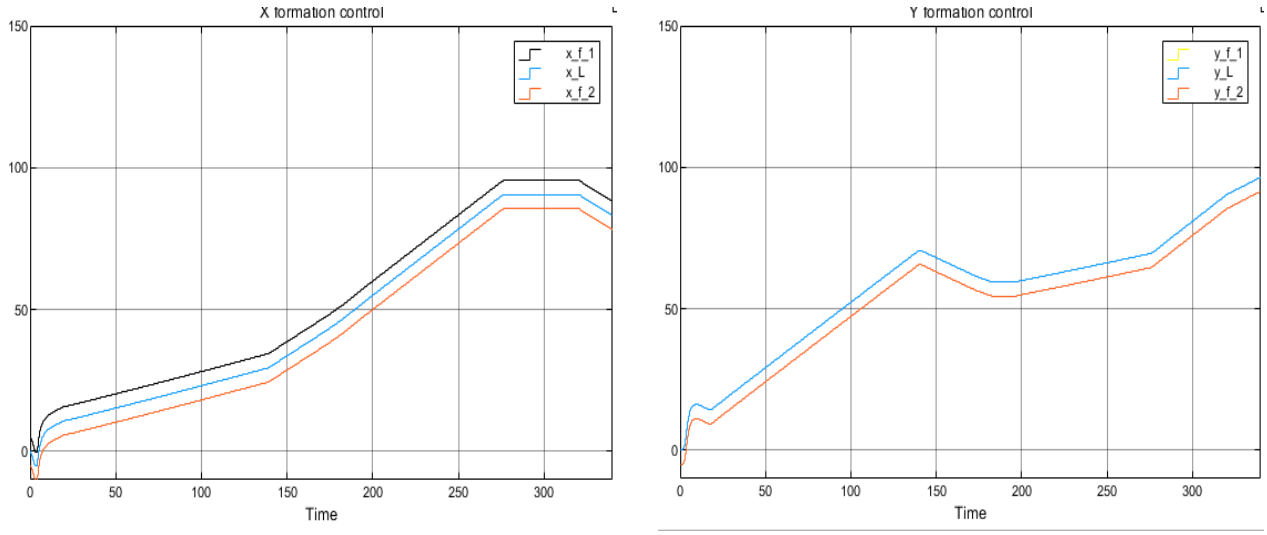

X formation control Y formation control

Figure IV-7: system response for the L-F formation control

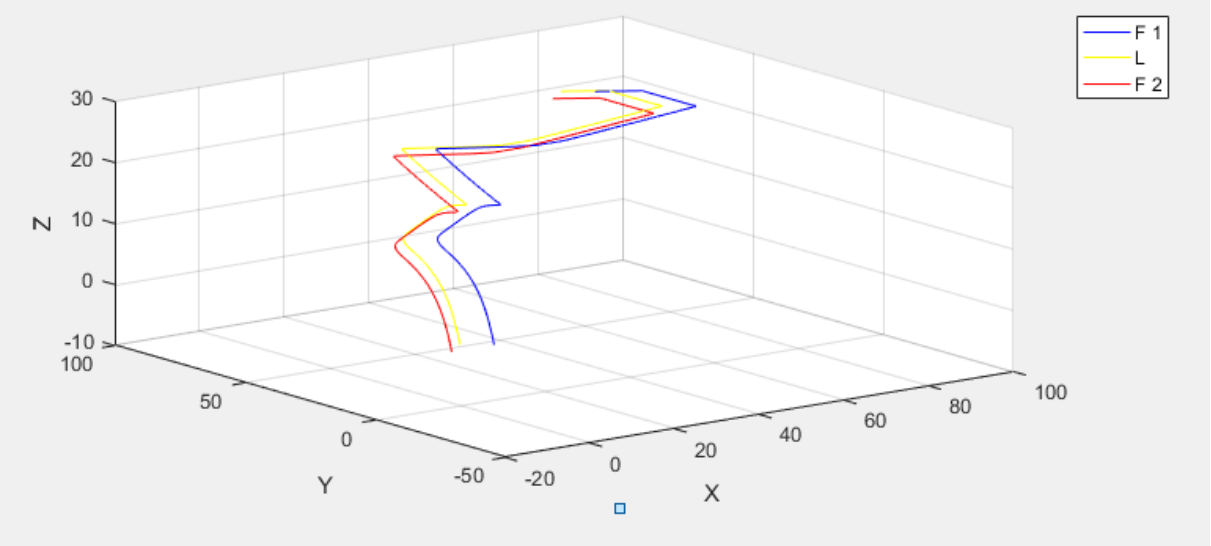

Figure IV-8: system response in 3D

Figure IV-9 shows that errors in all coordinates x and y were converged to zero.

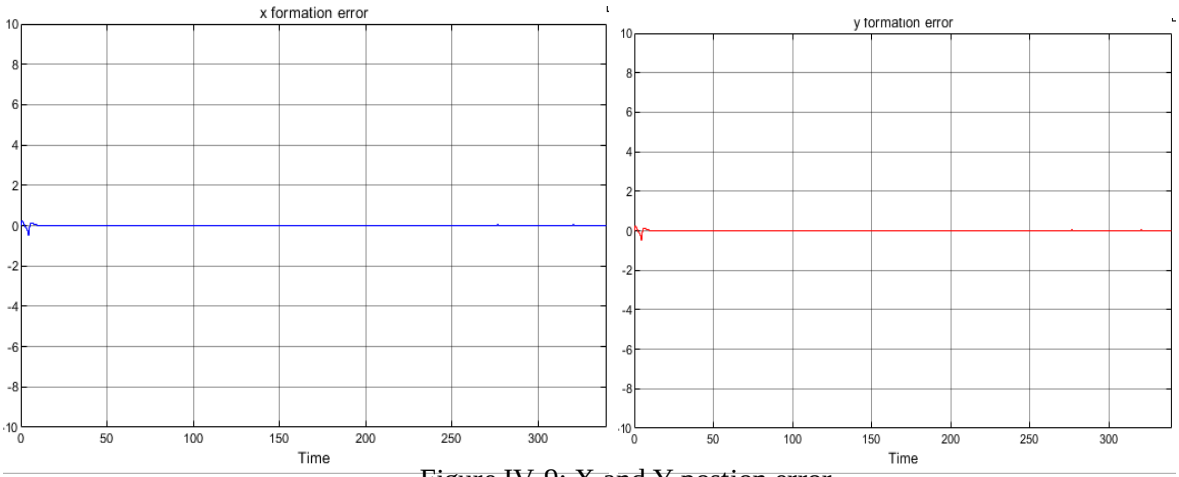

Figure IV-9: X and Y postion error

IV.5 CONCLUSION

This chapter investigated formation control strategy for multiple quadrotors UAVs based on leader-follower method. A SMC algorithm is used in designing the formation controller with acceleration used as the input to the follower controller. Simulation results show that the proposed controller succeeded to solve the formation control for the centralized Leader-followers case

GENERAL CONCLUSION

Unmanned aerial vehicles (UAVs) receive moreattention from researchers in both civilian and military applications.Especially quadrotor helicopters become vastly usedin most recent researches due to their capability of verticaltake-off and landing (VTOL). This characteristic helped themto successfully achieve their missions in many applicationssuch as search, exploration, reconnaissance, surveillance andfirefighting. However these tasks could be performed withone vehicle only, multiple vehicles will be more flexible, efficient and have more failure tolerance in performing the task.

As it’s mentioned using multiple UAVs is more effective but in the other hand controlling them is more complicated and difficult than controlling a single one. To solve this problem, the group of UAVs should maintain a certain formation shape with constantrelative distances.

Bibliography

1. **Bailey, Mark Willis.***Unmanned aerial vehicle path planning and image processing.* 2012.

2. **Wang, A.Azzam and Xinhua.***Quad rotor arial robot dynamic modeling andIn Informatics in Control, Automation and Robotics.* 2010.

3. **Schwing, Richard P.***Unmanned aerial vehicles-revolutionary tools in war and.* 2007.

4. **Wilson, JR.***UAV worldwide.* 2009.

5. **Timothy H Cox, Christopher J Nagy, Mark A Skoog, Ivan A Somers, and R warner.***Civil UAV capability assessment.* 2004.

6. **Luis Rodolfo Garcia, Alejandro Lopez and Claude Pegad.***Quad rotorcraft control.* 2012.

7.**Kendoul, Farid.***Survey of advances in guidance, navigation, and control of unmanned rotocraft systems.* 2012, Field Robotics.

8. **BOUABDALLAH, Samir.***design and control of quadrotors.* 2007.

9. **Siegwart, S. Bouabdallah and R.** 2005. In Robotics and Automation, 2005. ICRA 2005. Proceedings of the 2005 IEEE International Conference on, pages 2247-2252.

10. **Kushleyev, A.Kumar and Mellinger.***Towards a swarm of agile micro quadrotors.* Sydney, Australia : s.n., 2012.

11. **N. Michael, J. Fink and V. Kumar.***Robust global asymptotic attitude stabilization of a regid body by quaternion-based hybrid feedback.* Chaina : s.n., 2009.

12. **D'Andrea, Ritz and.***Carrying a flexible payload with multiple flying vehicles.* 2013.

13. **Saska, V. Vonasek and L. Preucil.***Coordination and navigation of heterogeneous mav-ugv formation localized by a hawk-eye like approach under a model predictive control scheme.* 2014.

14. **Choutri, K., Lagha, M., & Dala, L. (2019).** *Distributed Obstacles Avoidance For UAVs Formation Using Consensus-based Switching Topology. International Journal of Computing and Digital Systems, 8(2), 167-178.*

15. **Amr Nagaty, SAjad Saeedi, Carl Thibault and Howard Li** *Control and navigation framework for quadrotor helicopters.***.** 2013, intelligent and Robotic System.

16.**L Derafa, T Madani and A Benallegue.***Dynamic modelling and experimental identification of four rotors helicopter parameters.* 2006. ICIT 2006. IEEE International Conference.

17. **Regula, Gerely.***Formation control of autonomous aerial vehicles.* 2013.

18. **Bresciani, Tommaso.***Modelling, Identification and control of a Quadrotor Helicopter.* 2008.

19. **Tian, H. Miao and Y. C.** Dynamic robot path planning using an enhaced simulated annealing approach. 2013.

20. **Yilmaz, O. Cetin and G.** Sigmoid limiting functions and potential field based autonomous air refueling path planning for UAVs. 2014.

21. **A. Bakdi, A. Boutami and B. Bouzouia.** Optimal path planning and execution for mobile robots using genetic algorithm and adaptative fuzzy logic control. 2016.

22. **Lin, T.S. Wang and H.T.** An improvrd ant colony system algorithm for solving the IP traceback problem. 2016.

23. **Mingchang Wanga, b, Chunyu Zhua, Fengyan Wanga, Tingting Lia and Xinyue Zhangc.** Multi-factor of path planning based on an ant colony optimization algorithm. 2020.

24. **[En ligne] http://inndustry.blogspot.com//.**

25.Xiaolin Dai, Shuai Long, Zhiwen Zhang and Dawei Gong. 2019. *Mobile robot path planning based on Ant Colony Algorithm and A* heuristic method.*

26.Chen, Longwang Yue and Hanning. *Unmanned vehicle path planning* . 2019.

27.**Choutri, K., Lagha, M., Dala, L., & Lipatov, M. (2018, October)**. *Quadrotors UAVs swarming control under leader-followers formation. In 2018 22nd International Conference on System Theory, Control and Computing (ICSTCC) (pp. 794-799). IEEE.*

29.M. Turpin, N. Michael and V. Kumar.*Concurrent assignment and planning of trajectories for multiple robots.* 2014.

30. Hou, Zhicheng. *Modeling and formation controller design for multi-quadrotor systems with leader-follower configuration.* 2016**.**

31.**Choutri, K., Lagha, M., Dala, L., & Lipatov, M. (2017, April)**.*Quadrotors trajectory tracking using a differential flatness-quaternion based approach. In 2017 7th International Conference on Modeling, Simulation, and Applied Optimization (ICMSAO) (pp. 1-5). IEEE.*

32. **Choutri, K., Lagha, M., & Dala, L. (2020)**. *A Fully Autonomous Search and Rescue System Using Quadrotor UAV. International Journal of Computing and Digital Systems, 10, 2-12.*

33. **Choutri, K., Lagha, M., & Dala, L. (2019)**. *Multi-layered optimal navigation system for quadrotor UAV. Aircraft Engineering and Aerospace Technology.*

34. **Choutri, K., Mohand, L., & Dala, L**. *Design of search and rescue system using autonomous Multi-UAVs. Intelligent Decision Technologies, (Preprint), 1-12.*

35. **Choutri, K., Lagha, M., Dala, L., & Lipatov, M. (2018, March)**. *Linear Commands Comparison in a Real Time Simulation of a Quadrotors Unmanned Aerial Vehicle. In 2018 International Conference on Control, Automation and Diagnosis (ICCAD) (pp. 1-6). IEEE.*

APPENDIX A

SYSTEM MODELING DERIVATIONS

A.1 KINEMATICS MODEL

A.1.1 ROTATION MATRIX *R*

To describe the orientation of the quadrotor in space, 2 intermediate coordinate systemsneed to be defined; the vehicle-1 frame and the vehicle-2 frame together withthe previously defined inertial frame and body frame .

The inertial frame is rotated about its y-axis by the yaw angle to get the vehicle-1 frame. The transformation from the inertial frame to the vehicle-1 frame is given by

$$R_i^{v1}=\begin{bmatrix} cos\psi & sin\psi & 0 \\ -sin\psi & cos\psi & 0 \\ 0 & 0 & 1 \end{bmatrix} \quad \text{(A.1)}$$

The notation R_i^{v1} indicates a rotation from frame F_i which is the inertial frame toframe F_v1 which is the vehicle-1 frame.

The resulting frame v1 is then rotated by the pitch angle around its y-axis toresult in the vehicle-2 frame. The transformation from the vehicle-1 frame to the vehicle-2 frame is given by

$$R_{v1}^{v2}=\begin{bmatrix} cos\theta & 0 & sin\theta \\ 0 & 1 & 0 \\ sin\theta & 0 & cos\theta \end{bmatrix} \quad \text{(A.2)}$$

The last rotation is the rotation of the vehicle-2 frame about its x-axis to result in the body frame. The transformation from the vehicle-2 frame to the body frame is given by

$$R_{v2}^{b}=\begin{bmatrix} 1 & 0 & 0 \\ 0 & cos\Phi & sin\Phi \\ 0 & -sin\Phi & cos\Phi \end{bmatrix} \quad \text{(A.3)}$$

Finally the rotation matrix or transformation from the inertial frame to the bodyframe is given by

$$R_i^b=R_{v2}^b R_{v1}^{v2} R_i^{v1}$$

$$=\begin{bmatrix} 1 & 0 & 0 \\ 0 & cos\Phi & sin\Phi \\ 0 & -sin\Phi & cos\Phi \end{bmatrix}\begin{bmatrix} cos\theta & 0 & sin\theta \\ 0 & 1 & 0 \\ sin\theta & 0 & cos\theta \end{bmatrix}\begin{bmatrix} cos\psi & sin\psi & 0 \\ -sin\psi & cos\psi & 0 \\ 0 & 0 & 1 \end{bmatrix}$$

$$=\begin{bmatrix} c\phi c\theta & s\phi c\theta & -s\theta \\ c\phi s\theta s\psi - s\theta c\psi & s\phi s\theta s\psi + c\theta c\psi & c\theta s\psi \\ c\phi s\theta c\psi + s\phi s\psi & s\phi s\theta c\psi & c\theta c\psi \end{bmatrix} \quad \text{(A.4)}$$

where c and s denote cos and sin respectively. Note that due to the premultiplicationrule of rotation matrices, the order of rotation (followed by **Φ** followed by θ)is opposite to that of the order of multiplication (**Φ**followed by **Θ**followed by$\boldsymbol{\psi}$).

In order to get the rotation matrix that transforms the body frame to the inertial frame, the previous rotation matrix $R_i^b$is transposed, yielding

$$\text{R}={R_i^b}^T = R_b^i$$

$$R = \begin{bmatrix} c\theta c\psi & s\phi s\theta c\psi & c\phi s\theta c\psi \ + s\phi s\psi \\ c\theta s\psi & s\phi s\theta s\psi + c\theta c\psi & c\phi s\theta s\psi - s\theta c\psi \\ -s\theta & s\phi c\theta & c\phi c\theta \end{bmatrix} \tag{A.5}$$

A.1.2 EULER RATES

The transformation between the Euler rates $\dot{\eta} = \left[\dot{\theta}\dot{\phi}\dot{\psi}\right]^T{}_{\omega} = [pqr]^T$and angular body rates$\omega = [pqr]^T$ shown in Equation (3.2) is derived as follows [50]

$$\begin{bmatrix} p \\ q \\ r \end{bmatrix} = R\left(\dot{\phi}\right)\begin{bmatrix} \dot{\phi} \\ 0 \\ 0 \end{bmatrix} + R(\phi)R(\dot{\theta})\begin{bmatrix} 0 \\ \dot{\theta} \\ 0 \end{bmatrix} + R(\phi)R(\theta)R(\dot{\psi})\begin{bmatrix} 0 \\ 0 \\ \dot{\psi} \end{bmatrix} \tag{A.6}$$

Note that $\dot{\theta}, \dot{\phi}$ and $\dot{\psi}$are small thus$R(\dot{\theta}) = R\left(\dot{\phi}\right)$=$R(\dot{\psi})$=I

then

$$\begin{bmatrix} p \\ q \\ r \end{bmatrix} = \begin{bmatrix} \dot{\phi} \\ 0 \\ 0 \end{bmatrix} + \begin{bmatrix} 1 & 0 & 0 \\ 0 & cos\Phi & sin\Phi \\ 0 & -sin\Phi & cos\Phi \end{bmatrix}\begin{bmatrix} 0 \\ \dot{\theta} \\ 0 \end{bmatrix} + \begin{bmatrix} 1 & 0 & 0 \\ 0 & cos\Phi & sin\Phi \\ 0 & -sin\Phi & cos\Phi \end{bmatrix}\begin{bmatrix} cos\Theta & 0 & sin\Theta \\ 0 & 1 & 0 \\ sin\Theta & 0 & cos\Theta \end{bmatrix}\begin{bmatrix} 0 \\ 0 \\ \dot{\psi} \end{bmatrix}$$

$$= \begin{bmatrix} \dot{\phi} - sin\theta\dot{\psi} \\ cos\phi\dot{\theta} + sin\phi cos\theta\dot{\psi} \\ -sin\phi\dot{\theta} + cos\phi cos\theta\dot{\psi} \end{bmatrix} \tag{A.7}$$

$$= \begin{bmatrix} 1 & 0 & -sin\theta \\ 0 & cos\phi & sin\phi cos\theta \\ 0 & -sin\phi & cos\phi sin\theta \end{bmatrix}$$

APPENDIX 2

QUADROTOR PARAMETERS

This appendix contains the quadrotor parameters used in the simulations. These parameters are adopted from Tomasso's thesis (18).

parameter	Description	Value	Unit
I_{xx}	MOI about body frame's x-axis	8.1e-3	Kg.m^2
I_{yy}	MOI about body frame's y-axis	8.1e-3	Kg.m^2
I_{zz}	MOI about body frame's z-axis	14.2e-3	Kg.m^2
l	Moment arm	0.24	m
m	Quadrotor mass	1	kg
K_f	Aerodynamic force constant	6.3e-3	N.s^2
K_M	Aerodynamic moment constant	6.3e-3	N m.s^2
R_{mot}	Motor circuit resistance	0.6	Ω
L	Motorimpedance	15e-6	mN m/A
N	the gear box reduction ratio	5.6	–
η	gear box efficiency	0.9	–
J_M	the rotor moment of inertia around the motor axis	1.1×10^{-6}	N m s^2
J_{TP}	the total motor moment of inertia around the motor	104×10^{-6}	N m s^2
J_{TM}	the total motor moment of inertia around the motor	3.66×10^{-6}	N m s^2
J_p	the rotor moment of inertia around the propeller axis	72.2×10^{-6}	N m s^2

Table B.1: Quadrotor Parameters and Constants